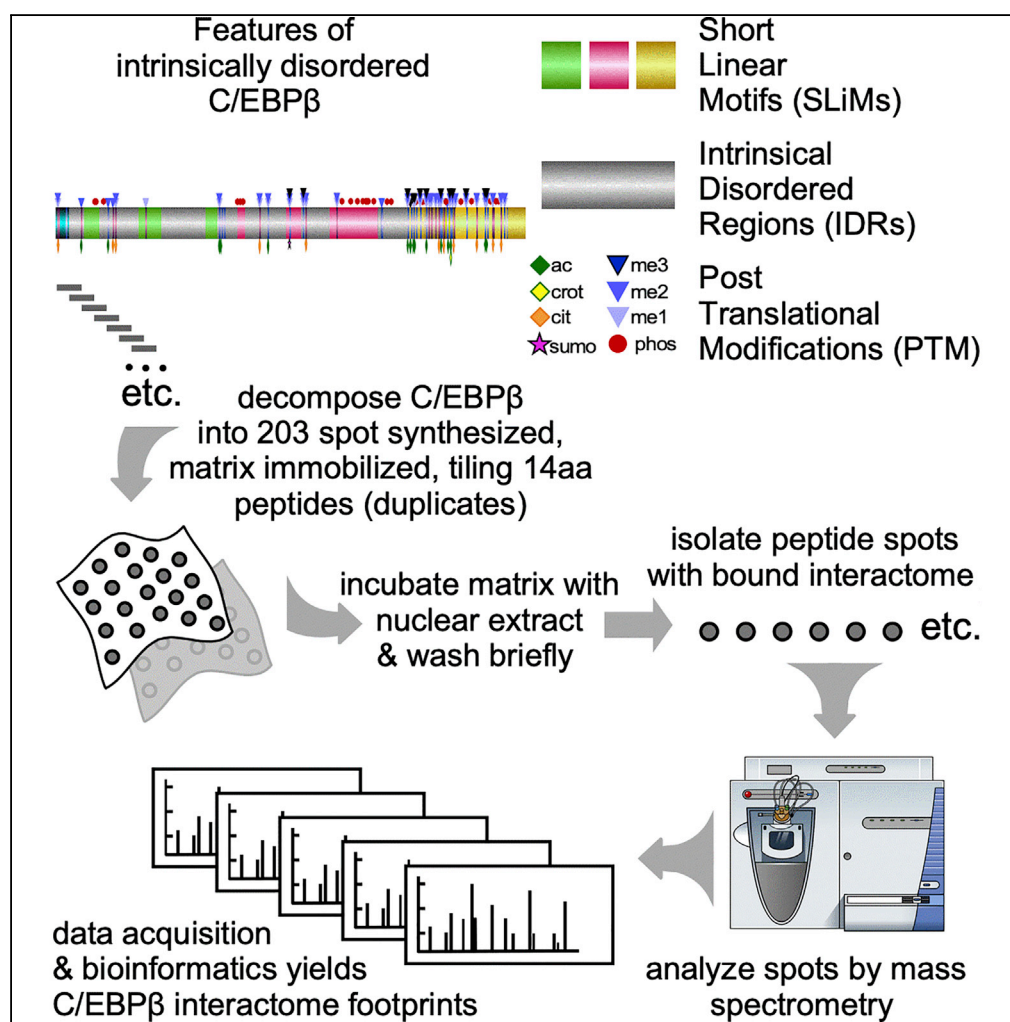


## Article

# PRISMA: Protein Interaction Screen on Peptide Matrix Reveals Interaction Footprints and Modifications-Dependent Interactome of Intrinsically Disordered C/EBP $\beta$



Gunnar Dittmar,  
Daniel Perez  
Hernandez,  
Elisabeth Kowenz-  
Leutz, ..., Jana  
Wolf, Ulf Reimer,  
Achim Leutz

gunnar.dittmar@lih.lu (G.D.)  
aleutz@mdc-berlin.de (A.L.)

**HIGHLIGHTS**

PRISMA yields a high-resolution SLiM- and PTM-based C/EBP $\beta$  interactome

Disclosure of intrinsically disordered protein hub functions and interaction networks

New connections between C/EBP $\beta$  and RNA processing, transcription elongation, MLL, NuRD

C/EBP $\beta$  interaction with TLE3 is regulated by arginine methylation

Dittmar et al., iScience 13,  
351–370  
March 29, 2019 © 2019 The  
Authors.  
[https://doi.org/10.1016/  
j.isci.2019.02.026](https://doi.org/10.1016/j.isci.2019.02.026)

## Article

# PRISMA: Protein Interaction Screen on Peptide Matrix Reveals Interaction Footprints and Modifications-Dependent Interactome of Intrinsically Disordered C/EBP $\beta$

Gunnar Dittmar,<sup>1,2,3,\*</sup> Daniel Perez Hernandez,<sup>2,3,6</sup> Elisabeth Kowenz-Leutz,<sup>2,6</sup> Marieluise Kirchner,<sup>2,3,6</sup> Günther Kahlert,<sup>2</sup> Radoslaw Wesolowski,<sup>2</sup> Katharina Baum,<sup>2</sup> Maria Knoblich,<sup>2</sup> Maria Hofstätter,<sup>2</sup> Arnaud Muller,<sup>1</sup> Jana Wolf,<sup>2</sup> Ulf Reimer,<sup>4</sup> and Achim Leutz<sup>2,5,7,\*</sup>

## SUMMARY

**CCAAT enhancer-binding protein beta (C/EBP $\beta$ ) is a pioneer transcription factor that specifies cell differentiation. C/EBP $\beta$  is intrinsically unstructured, a molecular feature common to many proteins involved in signal processing and epigenetics. The structure of C/EBP $\beta$  differs depending on alternative translation initiation and multiple post-translational modifications (PTM). Mutation of distinct PTM sites in C/EBP $\beta$  alters protein interactions and cell differentiation, suggesting that a C/EBP $\beta$  PTM indexing code determines epigenetic outcomes. Herein, we systematically explored the interactome of C/EBP $\beta$  using an array technique based on spot-synthesized C/EBP $\beta$ -derived linear tiling peptides with and without PTM, combined with mass spectrometric proteomic analysis of protein interactions. We identified interaction footprints of  $\sim$ 1,300 proteins in nuclear extracts, many with chromatin modifying, chromatin remodeling, and RNA processing functions. The results suggest that C/EBP $\beta$  acts as a multi-tasking molecular switchboard, integrating signal-dependent modifications and structural plasticity to orchestrate interactions with numerous protein complexes directing cell fate and function.**

## INTRODUCTION

CCAAT enhancer-binding proteins (C/EBP $\alpha$ ,  $\beta$ ,  $\delta$ ,  $\epsilon$ ) are basic leucine zipper (bZip) transcription factors that regulate chromatin structure and gene expression by dimerization and binding to cis-regulatory, palindromic 5'ATTGC·GCAAT3', or quasi-palindromic DNA sites in gene enhancers and promoters. Prototypic C/EBP $\beta$  is widely expressed, highly regulated at the post-transcriptional level, and integrated in many signaling events communicating extracellular cues to epigenetic changes, examples of which include adipogenesis, hematopoiesis, innate immunity, female fertility, skin function, apoptosis, and cellular senescence (Nerlov, 2008; Rodier and Campisi, 2011; Tsukada et al., 2011).

In early hematopoiesis and adipogenesis, C/EBP $\beta$  acts as a pioneering factor that orchestrates complex steps in cell fate commitment (Kajimura et al., 2009; Lichtinger et al., 2012; Muller et al., 1995; Ness et al., 1993; Siersbaek et al., 2011). C/EBP $\beta$  communicates with numerous other transcription factors, co-factors, histone modifiers, and chromatin remodeling complexes to alter the susceptibility of chromatin to the gene regulatory machinery. C/EBP $\beta$  induces lymphoid-myeloid *trans*-differentiation and accelerates acquisition of the induced pluripotent state by the Yamanaka set of reprogramming transcription factors (Di Stefano et al., 2016; Kowenz-Leutz and Leutz, 1999; Stoilova et al., 2013; Xie et al., 2004). The chromatin and gene regulatory functionality of C/EBP $\beta$  is linked to distinct regions and post-translational modifications (PTMs) that suspend auto-inhibition, direct the activity of C/EBP $\beta$ , and regulate recruitment of chromatin remodelers and writers of histone modifications (Kowenz-Leutz and Leutz, 1999; Kowenz-Leutz et al., 1994, 2010; Lee et al., 2010b; Mo et al., 2004; Pless et al., 2008; Siersbaek et al., 2011).

C/EBP $\beta$  functions are controlled by extracellular signaling cascades involving receptor tyrosine kinases, cytokine receptors, Ras GTPases, mitogen-activated protein kinases, and cyclic AMP and SMAD signaling, and by more complex conditions such as metabolic adaptation, inflammation, senescence, or stress responses (Nerlov, 2008; Rodier and Campisi, 2011; Tsukada et al., 2011). The complexity and diversity of C/EBP $\beta$  activities in various cell lineages raises the question of how a single transcription factor can

<sup>1</sup>Proteome and Genome Research Laboratory, Luxembourg Institute of Health, 1a Rue Thomas Edison, 1445 Strassen, Luxembourg

<sup>2</sup>Max Delbrück Center for Molecular Medicine, Robert-Roessle Strasse 10, 13125 Berlin, Germany

<sup>3</sup>BIH Core Facility Proteomics, Robert-Roessle Strasse 10, 10125 Berlin, Germany

<sup>4</sup>JPT Peptide Technologies GmbH, Volmerstrasse 5, 12489 Berlin, Germany

<sup>5</sup>Humboldt-University of Berlin, Institute of Biology, 10115 Berlin, Germany

<sup>6</sup>These authors contributed equally

<sup>7</sup>Lead Contact

\*Correspondence: [gunnar.dittmar@lih.lu](mailto:gunnar.dittmar@lih.lu) (G.D.), [aleutz@mdc-berlin.de](mailto:aleutz@mdc-berlin.de) (A.L.)  
<https://doi.org/10.1016/j.isci.2019.02.026>



participate in a multitude of regulatory events. Previous research suggested that the combinatorial outcome of post-transcriptional modifications and PTMs in conjunction with intrinsic structural plasticity enables the C/EBP $\beta$  protein to adopt a plethora of context- and signal-dependent states that facilitate a variety of interactions (Leutz et al., 2011; Nerlov, 2008; Tsukada et al., 2011).

Post-transcriptional regulation of C/EBP $\beta$  generates three isoforms (LAP\*, LAP, and LIP) by alternative translation initiation of the single-exon C/EBP $\beta$  transcript. As consecutive C/EBP $\beta$  start sites are positioned in the same reading frame, the isoforms vary in their gene regulatory N-terminal extensions but retain the same C-terminal dimerization and DNA-binding bZip domain (Wethmar et al., 2010). The diversity of C/EBP $\beta$  isoforms is further increased by numerous PTMs of amino acid side chains; in addition to phosphorylation of serine, threonine, and tyrosine residues, lysine acetylation and methylation also occurs, as does methylation of arginine. Enzymes responsible for PTM of C/EBP $\beta$  include CARM1/PRMT4, G9A/EHMT2, and CREBBP/KAT3A, all of which also serve as epigenetic histone code writers. The decoration of C/EBP $\beta$  by PTM alters its capacity to engage in protein-protein interactions (PPI) and to direct cell fate, suggesting that the signal-dependent C/EBP $\beta$  modification index reflects integration of various upstream signaling events to adjust its interactome and to determine its gene regulatory and epigenetic capacity (Leutz et al., 2011). The combination of translational modifications and PTMs may thus encrypt the dynamic interactome, with C/EBP $\beta$  being the keystone for a wide range of functional outcomes (Lee et al., 2010b; Sebastian et al., 2005; Sterneck et al., 1997; Stoilova et al., 2013).

The C-terminal third of C/EBP $\alpha$ ,  $\beta$ ,  $\delta$ ,  $\epsilon$  contains highly conserved DNA-binding and bZip domains that may dimerize within an extended *trans*-regulatory bZip network including C/EBP, AP-1, and ATF transcription factors. The N-terminal two-thirds region of the C/EBP primary structure is predicted as an intrinsically disordered region (IDR) (Miller, 2006). Phylogenetic analysis, nevertheless, suggests that the C/EBP N terminus also contains several highly conserved short peptide regions (CRs) that are enriched in amino acids with hydrophobic and bulky side chains. These CRs are discontinuous and separated by less conserved and family-specific regions of low complexity characterized by a predominance of small and polar amino acids (Leutz et al., 2011; Tsukada et al., 2011). Experimental studies involving a large number of deletions and CR/IDR shuffling mutants suggested a highly modular, context-dependent functionality of N-terminal C/EBP $\beta$  CRs (Kowenz-Leutz et al., 1994; Lee et al., 2010b; Leutz et al., 2011; Williams et al., 1995). Screening for interaction partners using N-terminally derived C/EBP $\beta$  peptides further supports the notion that many C/EBP $\beta$  interactions may occur in a modular and dynamic fashion that relies on molecular recognition features (MoRFs) and short linear peptide motifs (SLiMs) in combination with adjacent PTMs (Dunker et al., 1998; Leutz et al., 2011; Tompa et al., 2014; van der Lee et al., 2014; Wright and Dyson, 1999).

Based on previous observations of the modular structure and biological functionality of C/EBP $\beta$  peptide regions, we developed a novel technique to systematically explore the C/EBP $\beta$  interactome. Briefly, C/EBP $\beta$  was deconstructed into small linear peptides of 14 amino acids immobilized on a solid-phase matrix. The starting point for each peptide was shifted by four amino acids, creating a tiled peptide array covering the entire amino acid sequence of C/EBP $\beta$ . PTM-containing peptides were included according to recorded modifications and their position in the primary C/EBP $\beta$  structure. The matrix was incubated with nuclear extracts, and protein enrichment on individual peptide spots was identified and quantified by mass spectrometry. The assay, termed *protein interaction screen on peptide matrices* (PRISMA), revealed hundreds of C/EBP $\beta$ - and PTM-specific protein interactions that left footprints on C/EBP $\beta$ -derived peptides. Based on comparison with other affinity enrichment approaches, 45 protein complexes were predicted and several novel interactions with proteins and complexes were experimentally confirmed.

## RESULTS

### The C/EBP $\beta$ Peptide Matrix

The occurrence of novel PTMs on endogenous C/EBP $\beta$  was investigated by mass spectrometry of C/EBP $\beta$  immunoprecipitates derived from the human anaplastic lymphoma cell line SU-DHL1 that critically depends for growth and survival on C/EBP $\beta$  (Anastasov et al., 2010; Jundt et al., 2005). Over 90 PTMs were identified, which, combined with published data, suggested that more than 130 PTMs may occur on this protein, as summarized in Figure 1A (Table S1). To systematically explore the C/EBP $\beta$  interactome and its PTM-specific regulation, we developed the PRISMA technology, which is based on a solid matrix consisting of immobilized peptides spanning the entire primary structure of rat C/EBP $\beta$  (297 amino acids),

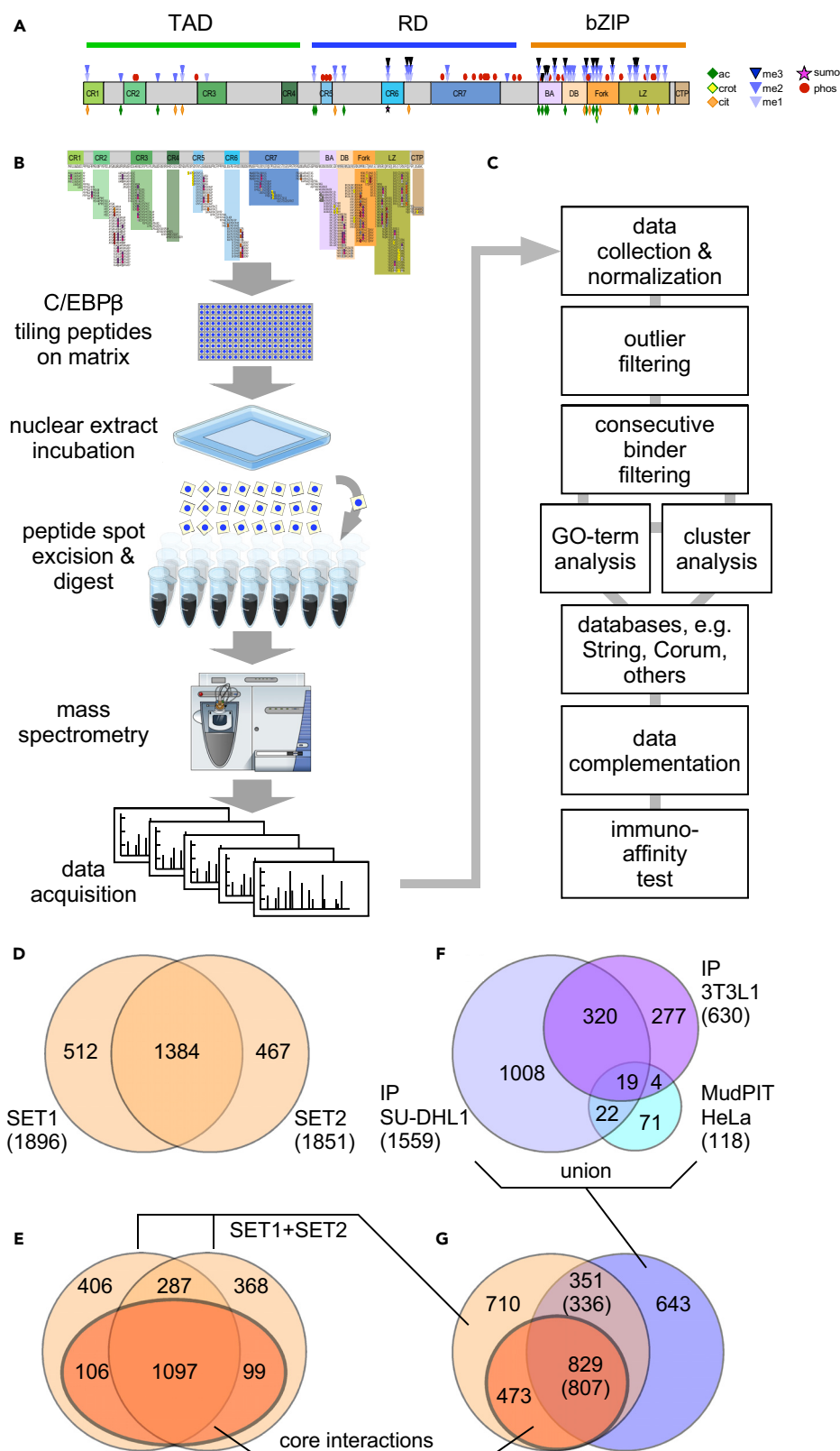




**Figure 1. Outline of PRISMA Screen and Comparison of Data**

- (A) Schematic representation of C/EBP $\beta$  and the distribution of known post-translational modifications. Conserved regions (CRs) are depicted in color, whereas intrinsic disordered regions are shown in gray.
- (B) Schematic description of the workflow of protein binding and data acquisition.
- (C) Workflow of data and proteomic analysis.
- (D) Overlap between the two replicates (SET1, SET2) of the PRISMA screen.
- (E) Number of proteins in the two PRISMA datasets that show consecutive peptide binding (core interactions, dark amber).
- (F) Overlap of three affinity-purification-based datasets of C/EBP $\beta$  interactors as described in the literature and combined with data obtained from a proteomic interaction screen in SU-DHL1 cells. Overlaps were determined using immunoprecipitation (IP) SU-DHL1 as reference dataset and thus the numbers add up to the size of this set only (see [Methods](#)).
- (G) Overlap of the PRISMA-derived C/EBP $\beta$  interactor datasets from (E) (union of SET1 and SET2, light amber) with core interactions (dark amber) from the union of the three datasets from (F) (blue). Overlaps are given using the PRISMA-derived data as reference datasets. The overlap count using the union of the datasets from (F) as a reference dataset is denoted in brackets.

as schematically depicted in [Figure 1B](#) and detailed in [Table S2](#). To cover all linear binding regions of the entire CEBP $\beta$  protein sequence, tiling peptides 14 amino acids long with an offset of mostly four amino acids were spot synthesized on a cellulose acetate matrix using Fmoc synthesis. As PTMs were previously shown to affect CEBP $\beta$  protein interactions and functionality, PTM peptides with S/T/Y-phosphorylation; K-acetylation; K-, R-methylation; and R-citrullination were included in the screen matrix. In total, the solid matrix contained 203 immobilized peptides, covering known and potential post-translational side chain modifications.

**The C/EBP $\beta$  PRISMA Screen**

To examine the linear CEBP $\beta$  interactome, two replicates of the peptide matrix were incubated with nuclear extracts of HeLa cells. HeLa cells express CEBP $\beta$ , and commercially available nuclear extracts have been used successfully by many research groups for the purification of biologically active proteins and protein complexes involved in gene regulation ([Figure 1B](#)). Individual peptide spots were excised and bound proteins proteolytically digested and analyzed by high-resolution mass spectrometry. In total, 406 analytical mass spectrometric 1-h runs were performed (approximately 17 days of measurement), and spectra were interpreted automatically using the MaxQuant software package.

Enrichment efficiency by PRISMA was examined by comparing the PRISMA intensity distribution with the total proteome of the nuclear extract. Approximately 5,100 proteins were identified and quantified in the nuclear cell extract using the intensity-based absolute quantification method ([Schwanhauser et al., 2011](#)). The copy number of proteins in the nuclear cell extract and the number of proteins bound in the PRISMA screen spans six orders of magnitude, suggesting that the identified binders are not biased toward highly abundant proteins ([Smits et al., 2013](#); [Figure S1](#)). Furthermore, the distribution of peptide or protein interactions was not attributed to physicochemical parameters of the peptides, as evidenced by comparison of the accumulated interaction intensities with peptide hydrophobicity (gravy index) and isoelectric points, which were determined for all non-modified PRISMA peptides. These results suggest that the PRISMA peptides on the matrix retained their specific protein-binding properties.

**Data Processing of C/EBP $\beta$  Peptide-Binding Proteins**

An initial inspection of the two replicate datasets revealed signal intensity variation of the interacting proteins. The two datasets were therefore integrated to increase robustness, as outlined in [Figure 1C](#) and as explained in the [Methods](#). The main source of variation arose from proteins that were identified only once on different peptide spots. This led to single (low confidence) and double (high confidence) identification categories for each peptide. The signal intensity for each protein was then normalized between 0 and 1 across all 203 matrix peptides. Individual peptides displayed large differences in binding partner profiles, further indicating the specificity of the interactions, because random binding would be expected to result in a more equal distribution of interacting proteins. Further analysis of the data showed that ~25% of the identified proteins bound to multiple C/EBP $\beta$  peptides across the array with low but varying intensity. Although these proteins may promiscuously bind to many distant peptides, some sections of the array showed much higher signals. To minimize noise from background binding, signal intensities for each

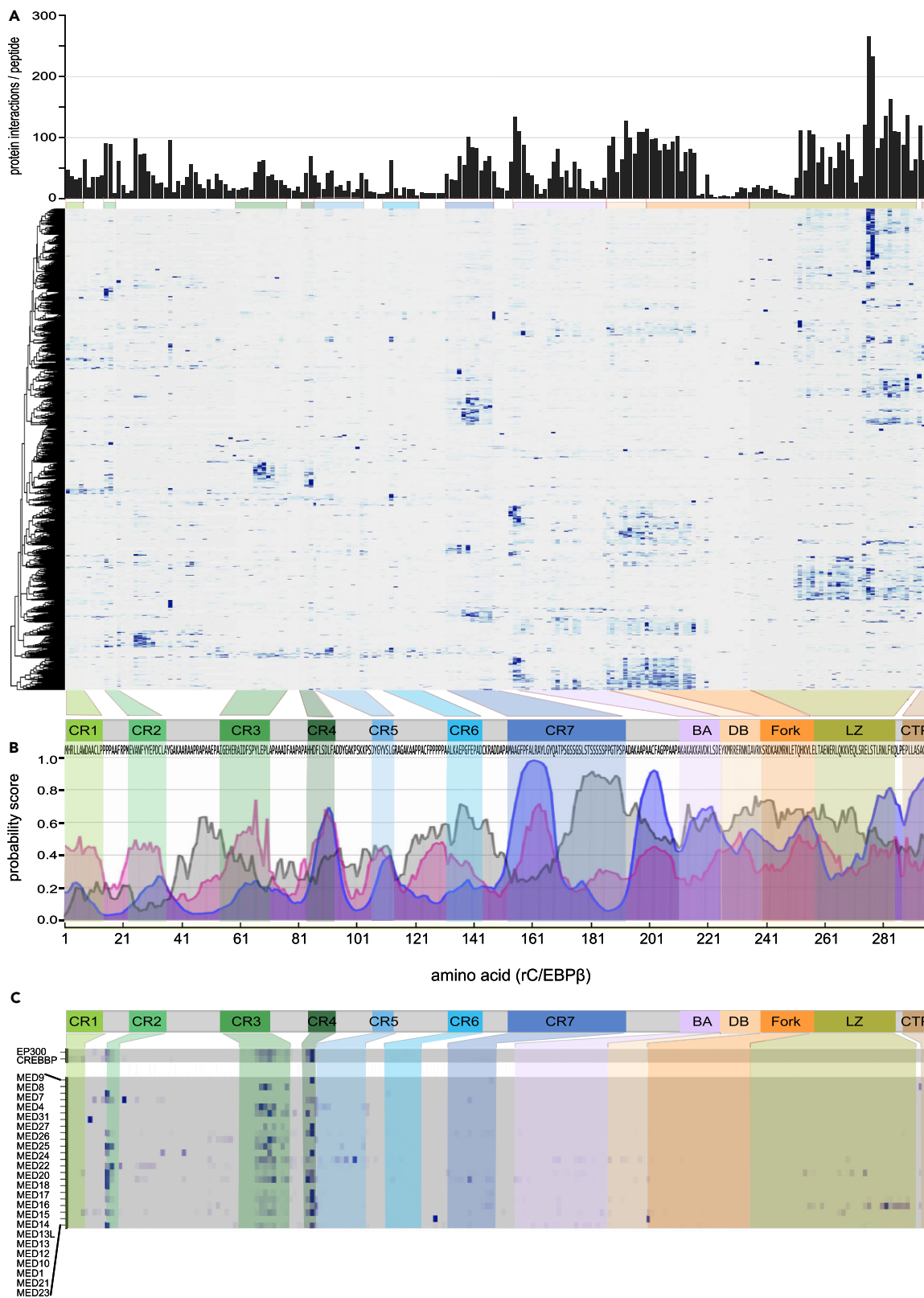


**Figure 2. Distribution of Protein Interactions Discovered by PRISMA**

(A) Heatmap of the normalized intensities of interaction partners. The bar graph (top) shows the distribution of accumulated protein interactions by normalized binding intensities for each peptide. The tiled peptides of C/EBP $\beta$  (below) are plotted on the horizontal axis, and proteins are shown on the vertical axis following non-supervised hierarchical clustering.

(B) Prediction of C/EBP $\beta$  interaction regions using "Anchor" (blue) and "MoRF" (magenta) bioinformatics tools and prediction of intrinsic disorder (gray) in relation to the schematic representation of C/EBP $\beta$  and the primary structure (bottom of A). Different conserved regions are colored as shown in Figure 1A.

(C) Heatmaps of selected complexes.

protein were filtered for binding above 90% of the protein's signal distribution (outlier filtering), removing all signals below this threshold. Another filtering criterion for discriminating the most robust interactors was based on the consecutive binding behavior of tiling peptides of the C/EBP $\beta$  primary structure. The rationale here is that by shifting the sequence of tiling peptides by four amino acids, some of the SLiMs and fractions thereof are included in more than one peptide. This may generate maximal binding signals for peptides containing optimal SLiM and adjacent supporting amino acids, and attenuated signals from neighboring peptides in which the particular SLiM is shifted or only partially included. We used this predicted binding behavior to stringently filter the dataset further to remove all proteins that failed the consecutive binding criterion (Figures 1D and 1E; see also Methods). In total, 2,363 interacting proteins were identified (Table S3), of which 1,384 proteins were detected in both replicates and 1,302 proteins fulfilled the consecutive binding criterion and were defined as C/EBP $\beta$  core interactions ( $\beta$ CI; Figure 1E).

**Validation of the PRISMA-Derived Dataset**

To assess the biological significance of data derived by PRISMA, we compared PRISMA data (SET1, SET2,  $\beta$ CI) to previously identified C/EBP $\beta$  interactome data, as shown in Figure 1F (Siersbaek et al., 2011; Steinberg et al., 2012). In addition, we performed pull-down experiments using C/EBP $\beta$  antibodies and SU-DHL1 cells that express a high amount of CEBP $\beta$  and analyzed the CEBP $\beta$  interactome by mass spectrometry (Table S4). In total, 1,369 proteins were significantly enriched in SU-DHL1 C/EBP $\beta$  samples compared with control samples using a false discovery rate (FDR) cutoff of 5%. The list of SU-DHL1 C/EBP $\beta$  interactors was included to extend the existing CEBP $\beta$  interaction datasets. The PRISMA core interaction data covered between 38% and 59% of the affinity-purification-based datasets (see Supplemental Information). Affinity purification-based datasets were then combined, and the overlap with PRISMA data was determined on the basis of their UniProt identifier entries, as shown in Figure 1G (see Methods). In total, 47% of data in all three sets were also found in the PRISMA core interactions, and 64% of PRISMA core interactions were also found in at least one of the other datasets. To estimate the FDR of the C/EBP $\beta$  interactor data detected by PRISMA, we employed the method proposed previously (D'Haeseleer and Church, 2004), which relies on comparing the intersections of protein interaction datasets to approximate the number of false-positive PPIs. We obtained FDRs of 11.2% and 13.9% for proteins detected in PRISMA replicates 1 and 2, respectively (SET1 and SET2 in Figures 1D and 1E; see Supplemental Information for details). FDRs were reduced to values below 4% when applying the filtering step leading to PRISMA core interactions. These results suggest that PRISMA data depict strong overlap and extensive coverage of the interactome related to native C/EBP $\beta$ . We conclude that the PRISMA method successfully extends the interactome data and serves as a resource for locating interaction footprints on C/EBPs.

**High-Resolution C/EBP $\beta$  Interactome Footprints**

The global protein interaction profile obtained from the C/EBP $\beta$  peptide matrix is depicted as a non-hierarchically clustered heatmap in Figure 2A. The numerical distribution of proteins identified by individual peptides is shown in the upper part of Figure 2A. Peptides representing the DNA-binding region (DB) and the C-terminal part of the leucine zipper (LZ) exhibit the highest number of protein interactions, yet locally enriched binding hotspots were also found with peptides from the N-terminal part of C/EBP $\beta$ .

Clusters of protein-peptide interactions tended to co-localize with regions predicted to undergo disorder-to-order transition during interaction with binding partners and coincide with the profile of conserved C/EBP $\beta$  regions (CR1–7), interaction and MoRF predictions (Disfani et al., 2012; Meszaros et al., 2009), as shown in Figure 2B. Predicted IDRs in the transactivating domain (CR1–4), IDR2 (between CR2 and CR3), and regulatory domain between CR7 and the basic or acidic region (IDR7) also displayed large numbers of interaction partners.

Next, PRISMA-derived data were compared with previously mapped C/EBP $\beta$ -interacting proteins. As shown in [Figure 2C](#), both co-activator acetyltransferases, CBP and P300 (KAT3A/KAT3B), generated highly similar interaction footprints in the transactivation regions CR4 (strongest binding) and CR3 (additional binding), with some residual binding in CR2. Both C/EBP $\beta$  and C/EBP $\delta$  have been shown to interact with CBP/p300, and the main interaction region encompasses the CBP Taz2 domain as well as CR3 and CR4 in both C/EBPs. Removal of CR3 or CR4, or mutation of a critical tyrosine residue in CR3 or the DLF motif in CR4 all abrogated interaction with Taz2 and subsequent transcriptional co-activation ([Kovacs et al., 2003](#); [Schwartz et al., 2003](#)). Previously published crystallographic data revealed that CR3/CR4 regions in C/EBP $\epsilon$  may adopt an L-shaped  $\alpha$ -helical structure that folds into the p300 Taz2 domain ([Bhaumik et al., 2014](#)), in agreement with the CBP/P300 protein footprints revealed by PRISMA ([Figure 2C](#)).

The multi-subunit Mediator (MED) complex ([Conaway and Conaway, 2013](#); [Jeronimo and Robert, 2017](#)) has also been reported to interact with C/EBP $\beta$  ([Mo et al., 2004](#)), and several MED components were identified in a previously published C/EBP $\beta$  interaction dataset ([Siersbaek et al., 2014](#)), as well as in the SU-DHL1 interactome presented here. As shown in [Figure 2C](#), PRISMA revealed 20 components of the multi-subunit MED complex that predominantly interact with CR2-, CR3-, and CR4-derived peptides from C/EBP $\beta$  TAD.

CR1 of the LAP\* C/EBP $\beta$  isoform was reported to specify conjugation by SUMO3 ([Eaton and Sealy, 2003](#)) and in accordance, PRISMA showed interaction between SUMO3 and CR1. CR1 also interacts with the Brg1/SMARCA4 ATPase of the SWI/SNF/BAF complex. Moreover, the Brg1-CR1 interaction is sensitive to methylation of arginine 3 ([Kowenz-Leutz et al., 2010](#)). Consistent with these results, PRISMA revealed interaction of Brg1 with the unmodified CR1 peptide, but not with the methylated peptide. Moreover, interactions with 10 additional protein components of BAF-SWI/SNF-type protein complexes were detected with various peptides of the C/EBP $\beta$  transactivation domain and the bZip domain, indicating multiple interactions between C/EBP $\beta$  and chromatin modifying complexes, as previously suggested ([Kowenz-Leutz and Leutz, 1999](#)).

### The Landscape of CEBP $\beta$ Protein Interactions

PRISMA data (SET1 and SET2) were inspected for enrichment of Gene Ontology (GO) terms, protein families, and protein domains. As shown in [Table 1](#), sorting of C/EBP $\beta$  interaction hits based on the quantity of terms resulted in exceedingly low Benjamini-Hochberg corrected FDRs (cutoff at a Benjamini-Hochberg corrected p value of 0.01) ([Finn et al., 2016, 2017](#); [Gene Ontology, 2015](#)). Strongly enriched terms included “nucleic acid binding” (745 hits), “gene expression” (611 hits), “protein binding” (534 hits), “regulation of transcription” (301 hits), “cell cycle” (211 hits), “RNA splicing” (172 hits), and several terms involving transcription, chromatin binding, and remodeling. Gene set enrichment analysis showed that approximately 25% of PRISMA-replicate-validated proteins (267) fell into categories that involve GO terms related to RNA processing (FDR  $5.63 \times 10^{-128}$ ). RNA-binding proteins that contain an RNP-1 RNA-binding domain fall into three classes that preferentially interact with the C/EBP $\beta$  bZip domain and the adjacent Fork and BA motifs, whereas a third group interacts with the CR2 region. A similar binding pattern was found for DEAD box helicases, a group of enzymes involved in ATP-driven conformational adjustment of ribonucleoprotein assembly.

Protein domain enrichment using InterPro and PFAM databases revealed nucleotide-binding proteins (102 hits), RNA-binding proteins (80 hits), armadillo, WD40, histone fold, and DEAD box domain proteins as major C/EBP $\beta$  interaction partners. The number of domain hits obtained using standard algorithms to search protein domain databases may be underrepresented, because manual curation of PRISMA data increased the number of hits for WD40 domain proteins (IPR017986: WD40 repeat, region) from 32 to 40, and the number of DEAD box proteins (IPR011545: DNA/RNA helicase; DEAD/DEAH box type, N-terminal) from 20 to 24.

The C/EBP $\beta$  structure is predicted to fold back onto itself, permitting intramolecular signaling, or to stretch out to allow contact with several interaction partners simultaneously ([Kowenz-Leutz et al., 1994](#); [Lee et al., 2010a](#); [Lynch et al., 2011](#)). A strong indication of the involvement of multiple contacts with interaction partners through adjacent or distant C/EBP $\beta$  regions is shown in [Figure S2A](#), which lists multivalent interactions, including potential interactions with different proteins of the same complex.

Enrichment Score	Pathway/Domain Description	Counts in PRISMA	FDR
GO: Biological Processes			
GO:0010467	Gene expression	611	$4.19 \times 10^{-103}$
GO:0006355	Regulation of transcription, DNA-templated	301	$1.27 \times 10^{-7}$
GO:0006396	RNA processing	267	$5.63 \times 10^{-128}$
GO:0007049	Cell cycle	211	$3.06 \times 10^{-31}$
GO:0008380	RNA splicing	172	$7.14 \times 10^{-106}$
GO:0051276	Chromosome organization	169	$1.16 \times 10^{-34}$
GO:0006461	Protein complex assembly	128	$4.17 \times 10^{-12}$
GO:0016568	Chromatin modification	89	$2.50 \times 10^{-13}$
GO:0051169	Nuclear transport	86	$9.46 \times 10^{-38}$
GO:0006281	DNA repair	84	$9.48 \times 10^{-17}$
GO: Molecular Function			
GO:0003676	Nucleic acid binding	745	$3.8 \times 10^{-199}$
GO:0003723	RNA binding	607	0E+00
GO:0005515	Protein binding	534	$1.92 \times 10^{-40}$
GO:0003677	DNA binding	269	$6.43 \times 10^{-17}$
GO:0005524	ATP binding	216	$2.82 \times 10^{-24}$
GO:0003682	Chromatin binding	94	$4.43 \times 10^{-18}$
GO:0003712	Transcription cofactor activity	81	$2.27 \times 10^{-9}$
GO:0008134	Transcription factor binding	66	$5.86 \times 10^{-9}$
GO:0019900	Kinase binding	61	$3.30 \times 10^{-6}$
GO:0004693	Cyclin-dependent protein serine/threonine kinase activity	17	$6.20 \times 10^{-10}$
GO: Cellular Component			
GO:0000785	Chromatin	103	$6.04 \times 10^{-31}$
GO:0005681	Spliceosomal complex	85	$5.10 \times 10^{-56}$
GO:0005643	Nuclear pore	32	$9.77 \times 10^{-19}$
GO:0030880	RNA polymerase complex	30	$2.98 \times 10^{-10}$
GO:0070603	SWI/SNF superfamily-type complex	28	$9.63 \times 10^{-14}$
GO:0034708	Methyltransferase complex	24	$4.86 \times 10^{-9}$
GO:0016592	Mediator complex	20	$3.98 \times 10^{-13}$
GO:0000178	Exosome (RNase complex)	12	$4.26 \times 10^{-9}$
GO:0016581	NuRD complex	11	$1.50 \times 10^{-9}$
GO:0016593	Cdc73/Paf1 complex	6	$1.01 \times 10^{-5}$

Table 1. C/EBP $\beta$  Interactome Enriched Gene Ontology (GO) Terms

(Continued on next page)

Enrichment Score	Pathway/Domain Description	Counts in PRISMA	FDR
Interpro Domains			
IPR027417	P loop containing nucleoside triphosphate hydrolase	102	$9.71 \times 10^{-30}$
IPR000504	RNA recognition motif domain	80	$8.77 \times 10^{-53}$
IPR005225	Small GTP-binding protein domain	41	$2.11 \times 10^{-13}$
IPR016024	Armadillo-type fold	34	$1.69 \times 10^{-11}$
IPR017986	WD40-repeat-containing domain	32	$6.78 \times 10^{-10}$
IPR009072	Histone-fold	27	$3.89 \times 10^{-9}$
IPR001650	Helicase, C-terminal	23	$1.94 \times 10^{-14}$
IPR011989	Armadillo-like helical	21	$5.11 \times 10^{-6}$
IPR011545	DEAD/DEAH box helicase domain	20	$2.11 \times 10^{-13}$
IPR002041	Ran GTPase	20	$5.34 \times 10^{-12}$
PFAM Domains			
PF00076	RNA recognition motif. (also called RRM, RBD, or RNP domain)	72	$4.32 \times 10^{-49}$
PF00071	Ras family	31	$8.17 \times 10^{-9}$
PF00400	WD domain, G-beta repeat	29	$1.38 \times 10^{-10}$
PF00271	Helicase-conserved C-terminal domain	23	$2.27 \times 10^{-14}$
PF00125	Core histone H2A/H2B/H3/H4	23	$1.89 \times 10^{-9}$
PF00270	DEAD/DEAH box helicase	20	$2.63 \times 10^{-13}$
PF00013	KH domain	10	$1.36 \times 10^{-6}$
PF00244	14-3-3 protein	6	$2.32 \times 10^{-4}$
PF01423	LSM domain	9	$2.32 \times 10^{-4}$
PF00538	Linker histone H1 and H5 family	5	$4.50 \times 10^{-4}$

Table 1. Continued

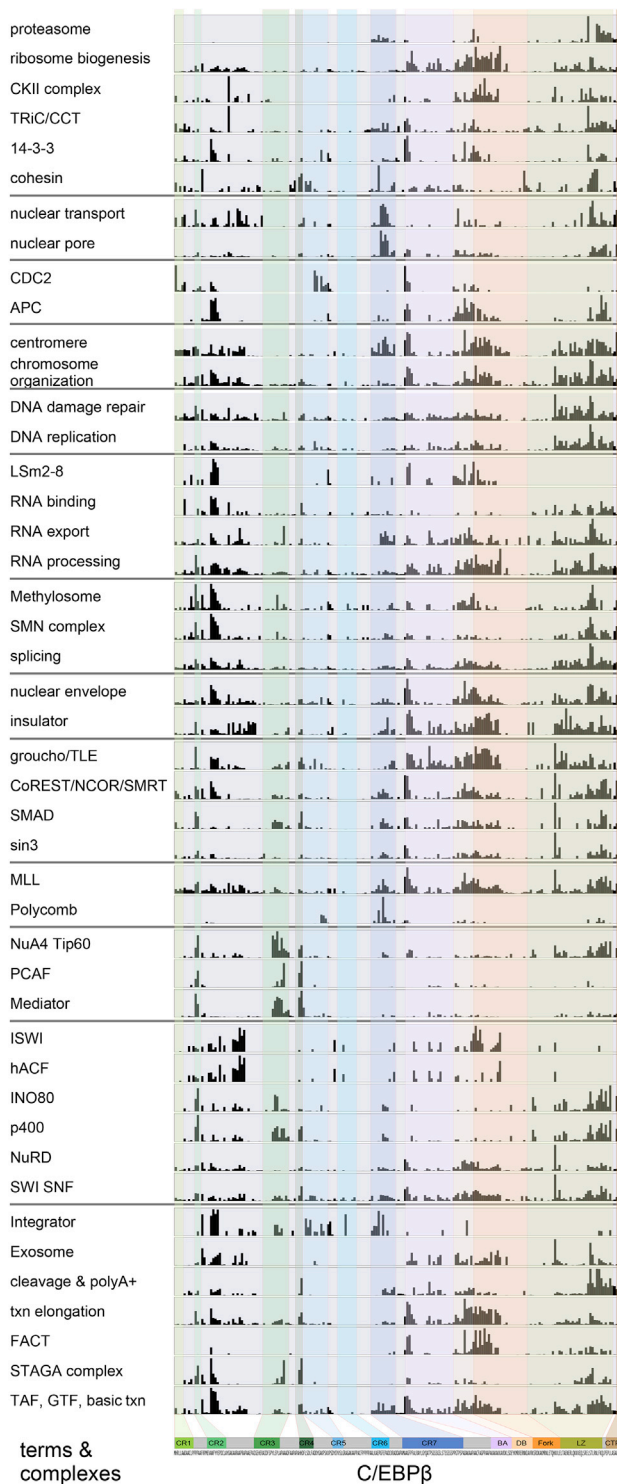
Discrete parts of the C/EBP $\beta$  primary structure have previously been assigned to different biochemical or cellular functions. Protein binding data from different C/EBP $\beta$  regions were extracted and GO term analysis performed for each of the regions to map structure-function relationships, as shown in Figure S2B. Some functional attributions displayed partition over several regions of C/EBP $\beta$  (regulation of gene expression, RNA splicing), whereas others are more localized to distinct regions. For example, basic regions and DB show strong enrichment for "regulation of mitotic cell cycle processes" or "nuclear export," whereas "nuclear import" is associated with CR5, CR7, IR7, and LZ. The C-terminal region of C/EBP $\beta$  is involved in the majority of GO terms, whereas transcription factor co-activator functions are mainly associated with N-terminal activation of CR2, CR3, CR4, and IR7.

### C/EBP $\beta$ -Interacting Protein Complexes

Next, PRISMA data were analyzed for potential enrichment of large protein complexes interacting with CEBP $\beta$ . In addition to anticipated C/EBP $\beta$ -interacting complexes such as the basic RNA polymerase II (RNAPII) transcription machinery or MED, previously unknown interrelations became apparent. These included potential complexes involved in the RNA transcript processing machinery responsible for transcript capping, splicing, termination, and polyadenylation. Interactions included 3'-end processing, cleavage, and polyadenylating factor (CPSF1, 3, 7, 30, and 100), and several components of the Integrator complex involved in small nuclear RNA (snRNA) expression and the RNA exosome (EXOSC2, 4, 6, 7, 8, 9,



**A**



**B**

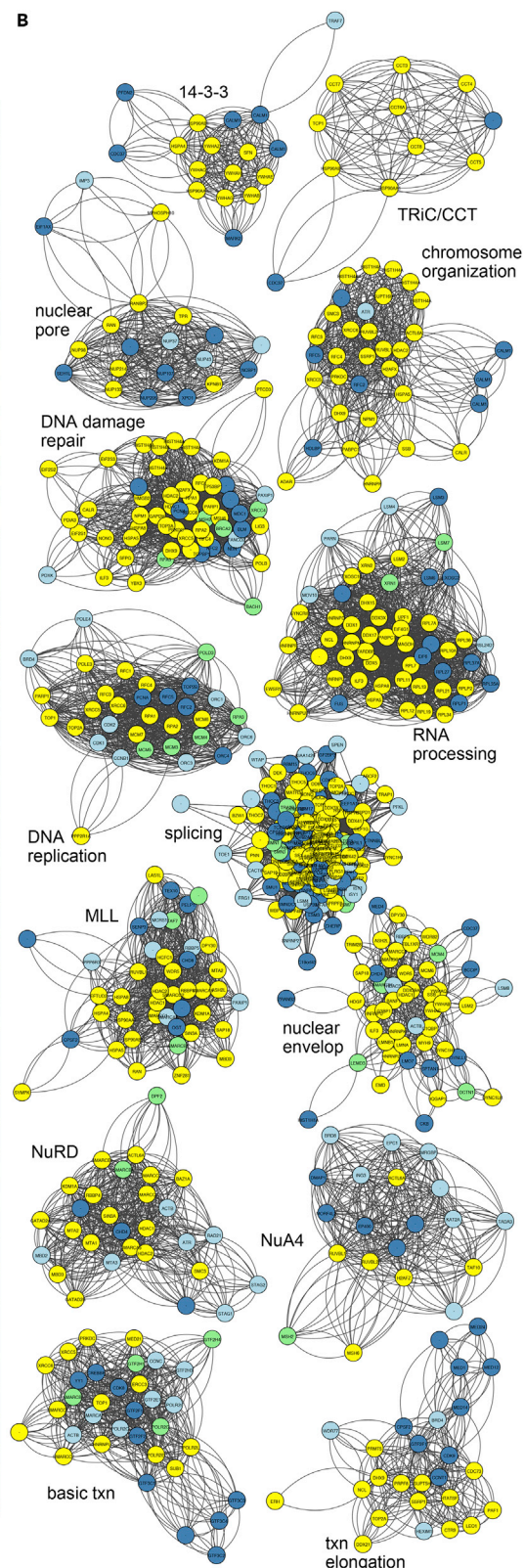


### Figure 3. PRISMA-Based Prediction of Protein Complexes Interacting with C/EBP $\beta$

(A) Bar graphs of accumulated normalized intensities for 45 selected complexes. Based on CORUM database protein complex annotations, the corresponding normalized intensities of proteins identified by PRISMA were extracted and plotted.

(B) Network representation of 14 potential complexes identified. Nodes are color coded according to their detection in PRISMA and SU-DHL1 IP experiments (yellow, detected in IP and PRISMA; green, detected in IP; dark blue, detected in the PRISMA core set; light blue, detected in PRISMA SET1 and SET2).

and 10). Furthermore, many components of the nuclear pore and associated adapter complexes were identified. In addition, components of the transcript export THO-TREX complex, including THO1, 2, 3, 5, 6, 7, Aly, DDX39, and the THO-TREX-associated mRNA export factors Nxf1-Nxt1 were identified, along with a large number of heterogeneous nuclear ribonucleoproteins that may couple transcript splicing, maturation, and the formation of messenger ribonucleoprotein particles. Taken together, these data imply the existence of a previously unknown connection between CEBP $\beta$  and several steps involved in transcript generation, processing, maturation, and transport (Muller-McNicol and Neugebauer, 2013; Wickramasinghe and Laskey, 2015).

Proteins co-occurring in both the PRISMA and SU-DHL1 proteomic data were then systematically explored to identify soluble protein complexes listed in the CORUM database (March 6, 2017) using the g:Profiler bioinformatics toolkit (Reimand et al., 2016; Ruepp et al., 2010). A list of 1,432 human protein complexes built from 2,678 proteins (single UniProt identifier; ID) was derived after removal of redundant and non-human complex entries. Proteins listed in PRISMA replicates (SET1 + SET2) and protein interactions derived from SU-DHL1 IP-mass spectrometry data were matched by UniProt and gene name ID using Perseus version 1.5.2.4 (Tyanova et al., 2016). Redundant gene names and isoform entries were merged into a single UniProt ID for each protein. Altogether, 816 proteins of the PRISMA-derived dataset and 490 proteins of the IP SU-DHL1 dataset were included in any of the 1,432 CORUM complexes. The 1,432 CORUM complexes were then ranked by a combination of two criteria: (1) the percentage of proteins in complexes obtained by PRISMA and (2) deviation from randomness of the coverage of the complexes obtained by PRISMA and SU-DHL1 (p values with CORUM background, see Supplemental Information for details). Considering only complexes sharing at least one protein with the PRISMA dataset and which have at least three overlaps with PRISMA and SU-DHL1 data resulted in a ranked list of 417 candidate complexes (see Figure S3 and Table S5). Whenever possible, complexes were grouped into categories indicating functional connections, such as DNA repair, nuclear pore, or centromere, in addition to well-characterized multi-subunit complexes, such as MED, SWI/SNF, MLL, nucleosome remodeling deacetylase (NuRD), and others. As shown in Figure 3A, 45 multi-protein complexes and categories were extracted, and normalized protein interaction values at any of the 203 C/EBP $\beta$  peptides were summed over all instances of the category in the list and depicted as a bar plot to visualize the distribution of interaction sites of different categories or complexes in relation to the C/EBP $\beta$  primary structure. These 45 entities were composed of 30 complexes or categories representing the full upper quartile of the ranked complex list (i.e., up to rank 104, Table S5, with minor exceptions, Figure S3), together with 15 lower-ranking functional counterparts. Figure 3B shows prominent node-link diagrams of a selection of 14 multi-protein complexes among the highest ranking categories that share many proteins identified by both PRISMA and SU-DHL1 immunoprecipitation methods.

### Validation of Region- and PTM-Specific C/EBP $\beta$ Interactions

Next, conventional protein pull-down, immunoprecipitation, and immunoblotting analysis were used in combination with CEBP $\beta$  mutants to validate data from the PRISMA-derived interactome (Figure 4). According to PRISMA, the nuclear factor kappa B subunit RelA, the signal transducer and activator of transcription STAT3, and the nuclear pore complex protein NUP50/NPAP60L predominantly interacted with peptides located in CR7. Bacterially expressed GST-C/EBP $\beta$  constructs were probed with HEK293 extracts to examine RelA and NUP50/NPAP60L interactions. As shown in Figures 4B and 4D (lower panels) affinity capture with GST-CEBP $\beta$  constructs or co-immunoprecipitation of STAT3 with the C/EBP $\beta$  mutant protein lacking CR7 and subsequent immunoblotting confirmed CR7 as the interaction site for all three proteins.

The histone acetyltransferase GCN5 of the SAGA complex and the DNA methyltransferase-associated protein DMAP1 of the NuA4/TIP60 acetyltransferase complex are involved in a wide variety of developmental and genome regulatory activities, including transcription, DNA repair, DNA methylation, and chromatin remodeling (Mohan et al., 2006; Weake and Workman, 2012). DMAP1 and GCN5 engage in major binding

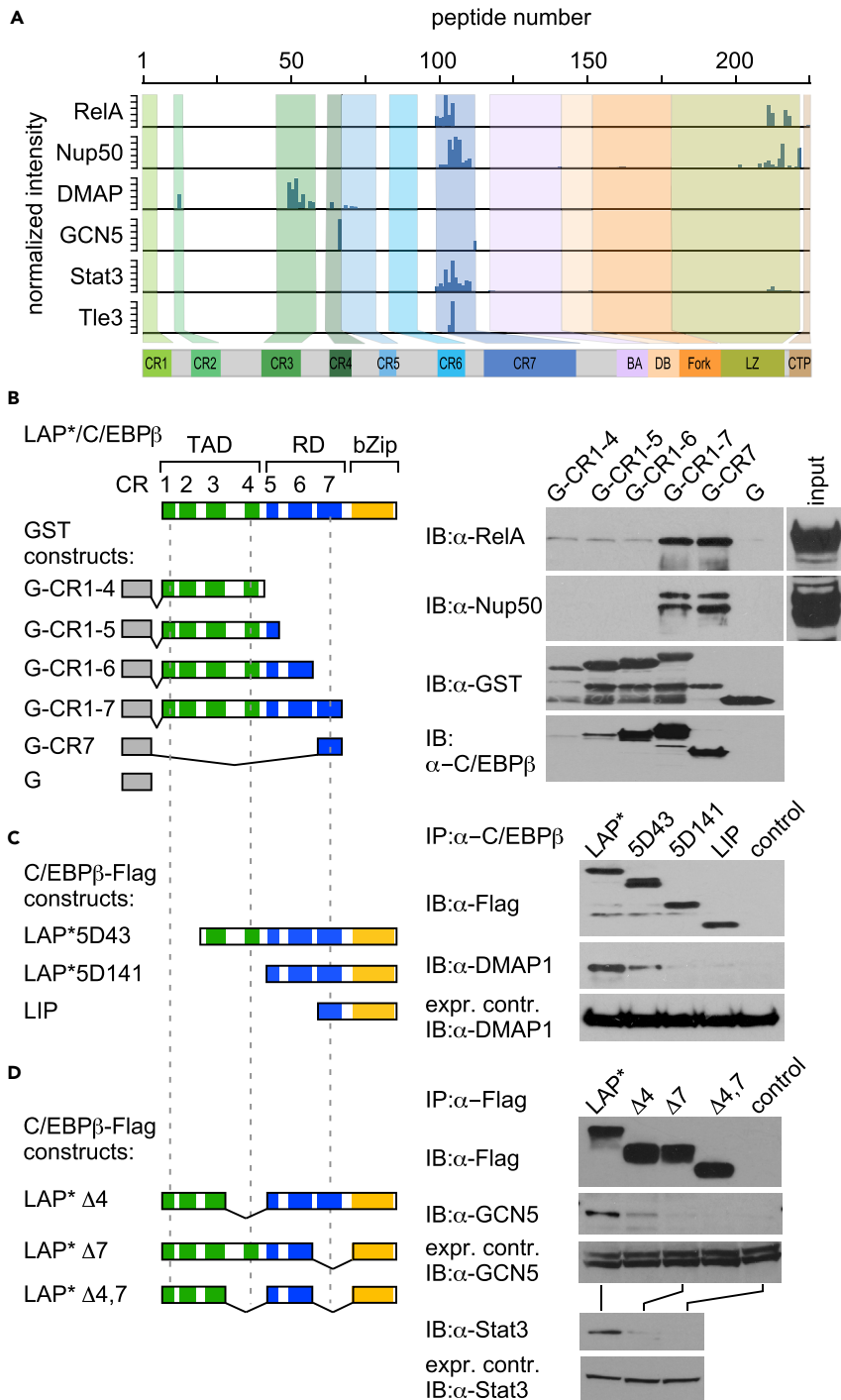


**Figure 4. Validation of Site-Specific Interactions with C/EBPβ**

(A) Accumulated binding intensities of interaction partners (indicated on the left) from the PRISMA screen. Bar graphs indicate interactions according to the peptide position in C/EBPβ, as schematically shown underneath.

(B) Top, left: Color-coded scheme of the C/EBPβ protein with dashed lines to aid comparison of constructs shown in (B–D). Top, right: Immunoblots (right) showing interaction of RelA and Nup50/NPAP60L of HEK293T cell lysates with bacterially expressed GST-C/EBPβ constructs. Integrity of GST-C/EBPβ constructs was examined by immunoblotting (as indicated). GST constructs were probed with anti-GST and a polyclonal C/EBPβ antibody that preferentially, but not exclusively, recognizes CR7 as a major epitope. The most intense signals of RelA and Nup50/NPAP60L are associated with the presence of the CR7 region of C/EBPβ. A, antibody; IP, immunoprecipitation; IB, immunoblotting.

**Figure 4. Continued**

(C) Co-immunoprecipitation of FLAG-tagged LAP\* C/EBP $\beta$  or three N-terminal C/EBP $\beta$  deletion mutants, followed by immunoblot detection of co-precipitated DMAP1 from HEK293 cells.

(D) Immunoprecipitation of HEK293 cells expressing LAP\* and three different internal deletion mutants of C/EBP $\beta$  followed by immunoblot detection of GCN5 and Stat3.

to CR3 and CR4, respectively, and minor binding elsewhere in C/EBP $\beta$ . Various C-terminally FLAG-tagged C/EBP $\beta$  mutant constructs lacking CR1, CR2 (5D43), the entire TAD (5D141), CR4 (LAP\* $\Delta$ 4), CR7 (LAP\* $\Delta$ 7), or both CR4 and CR7 (LAP\* $\Delta$ 4,7) were expressed in HEK293 cells to examine selective and multi-site interaction with resident DMAP1/GCN5 or their respective complexes. As shown in Figures 4C and 4D, pull-down and immunoblotting revealed that removal of the DMAP1 minor binding site in CR2 partially abrogated the interaction and removal of binding to CR3 completely abrogated the interaction. Similarly, removal of the binding site for GCN5 located in CR4 strongly affected GCN5 association and deletion of the binding site in CR7 entirely abolished binding to C/EBP $\beta$ .

**The Impact of PTMs on C/EBP $\beta$ -Mediated Interactions**

Detection of PTM-dependent protein interactions in linear C/EBP $\beta$  peptides was a major objective for the development of the PRISMA screening method. Protein binding to each PRISMA peptide and its PTM-modified versions were therefore examined. The binding signal for each protein was normalized against the signal from the corresponding unmodified peptide to compare enhanced or reduced binding. Interacting proteins were then clustered, as shown in Figure S4. Depending on PTM, as exemplified in Figure 5A, interactions fell into the following four categories: (1) generally repressed binding, (2) PTM-independent binding, (3) PTM-specific binding, and (4) generally enhanced binding. Most of the identified binding partners were indifferent to the type of PTM and were classified as binding proteins that may recognize parts of the peptide sequences. Generally enhanced binding may in part relate to the fact that many PTMs increase hydrophobicity and may thus enhance interactions non-specifically. The most interesting binding partners are expected to be found in the last two categories and represent proteins that are disturbed by any PTM in the peptide or represent interaction partners that were attracted or repelled by a particular PTM. Examples of the latter are the NuA4/TIP60 complex components DMAP1 and YEATS4, both binding to CR3, or RelA and the transducin-like enhancer protein TLE3 binding to CR7, which depends on the methylation status of arginine residues that were subsequently examined.

The transactivation region CR3 (residues 53–68: AIGEHERAIDFSPYLE) contains an arginine residue that is conserved in C/EBP $\beta$ , but not in C/EBP $\alpha$ , $\delta$ , $\epsilon$ , and was previously found to be methylated (Leutz et al., 2011). The PRISMA data suggested that DMAP1 and YEATS4 binding to CR3 depended on methylation of R59. Another interaction hotspot was mapped to the start site of the highly conserved, alternatively initiated LIP C/EBP $\beta$  isoform that also represents part of the regulatory region CR7 (residues 158–170: PPFALRAYLGYQAT). The respective arginine residues in both chicken (R60, R193) and rat (R58, R162) were previously found to be methylated. Mutation of the equivalent amino acid residue to alanine or leucine in chicken C/EBP $\beta$  strongly altered transcriptional activity, suggesting that the methylation status of the conserved arginine in CR7 may be critical (Leutz et al., 2011). Wild-type (WT) C/EBP $\beta$ , methylation-defective R60A and R193A, and methylation-mimicking R60L and R193L constructs were subjected to co-immunoprecipitation to compare alterations in binding, as shown in Figure 5B. As suggested by PRISMA, interaction of all four proteins with C/EBP $\beta$  was sensitive to the amino acid side chain configuration at the respective arginine positions, demonstrating both amino acid and PTM specificities, in addition to evolutionary conservation of chicken and rat C/EBP $\beta$  interactions. Binding of YEATS4 or DMAP1 to C/EBP $\beta$  was enhanced or tolerated by the R60L exchange, but not the R60A exchange, respectively, confirming the side chain specificity and preference for increased side chain hydrophobicity. RelA binding to the R193A mutant was slightly enhanced when compared with WT or reduced by the R193L mutant, respectively, confirming avoidance of the methylated, more hydrophobic PRISMA peptide. By contrast, the TLE3 co-repressor (Agarwal et al., 2015) favored binding to the R193L mutant, suggesting that the increase in hydrophobicity by methylation of the arginine side chain, but not the positive charge, was important for interaction with TLE3. Pull down of TLE3 by immunoprecipitation confirmed preferential binding of C/EBP $\beta$ R193L, as shown in Figure 5C. Next, we performed methylation assays with the protein arginine methyltransferase PRMT4/CARM1 and C/EBP $\beta$  peptides, as shown in Figure 5D. C/EBP $\beta$ R193 was identified as a methylation target in CR7, in addition to the previously described R3 in CR1 (Kowenz-Leutz et al., 2010). Co-immunoprecipitation of TLE3 together with WT C/EBP $\beta$  was dependent on co-expression of PRMT4/CARM1 (Figure 5E). Importantly, and irrespective of co-expressed



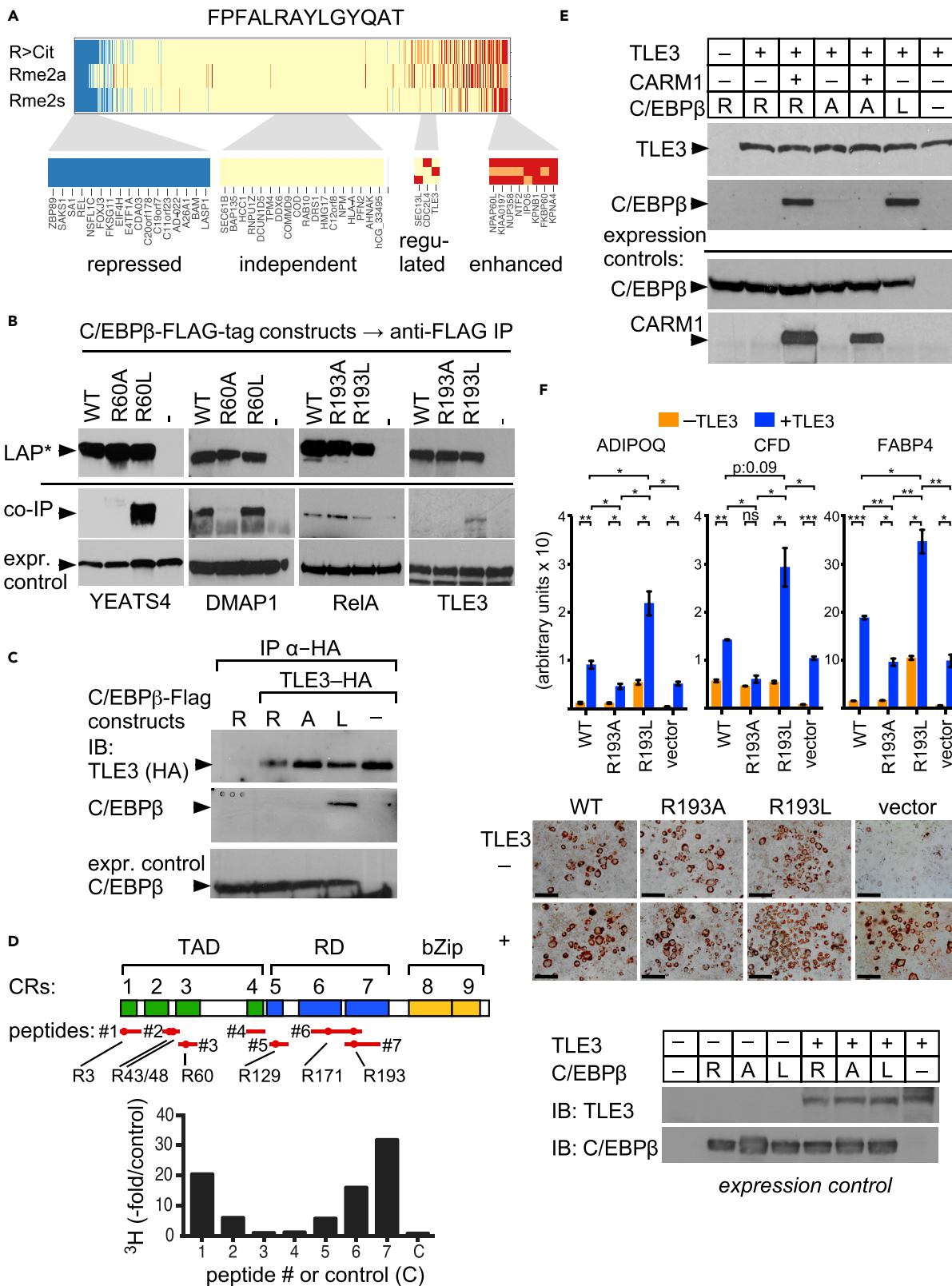


### Figure 5. PTM-Specific C/EBP $\beta$ Interactions

(A) PTM-dependent protein binding to PPFALRAYLGYQAT peptides of C/EBP $\beta$  CR7. Normalized binding intensity relative to the unmodified peptide. Four binding categories are considered: proteins with reduced binding by any PTM (repressed, blue, far left), proteins not responding to modifications on C/EBP $\beta$  (independent, yellow, middle), proteins with PTM-specific binding (regulated, yellow-red, small), and enhanced binding by any PTM (enhanced, red, far right).

(B) Immunoprecipitation (IP) from transfected HEK293T cell lysates: FLAG-tagged C/EBP $\beta$  wild-type (WT) or mutants, as indicated, abrogating C/EBP $\beta$  R60A; R193A) or mimicking (C/EBP $\beta$  R60L, R193L) methylation. Co-immunoprecipitation (colP) of endogenous YEATS4 and DMAP1 detected by immunoblotting. YEATS4 and DMAP1 bind to C/EBP $\beta$ R60L and failed to bind to the R60A C/EBP $\beta$  mutant. RelA favors WT or C/EBP $\beta$ R193A binding over R193L. TLE3 preferentially binds to C/EBP $\beta$ R193L. Underneath: Expression controls of endogenous YEATS4, DMAP1, RelA, and TLE3.

(C) colP of WT and mutant C/EBP $\beta$ , as indicated, with hemagglutinin (HA)-tagged TLE3. C/EBP $\beta$ R193L, but not WT or R193A, co-IPs with TLE3.

(D) *In vitro* methylation of C/EBP $\beta$  peptides by CARM1. Scheme of C/EBP $\beta$  with approximate positions of peptides and R-residues indicated by red bars and dots; R residue sequence positions underneath. Bar graphs show peptide-specific incorporation of methyl group from donor S-adenosyl-L-[methyl-<sup>3</sup>H] methionine.

(E) colP of C/EBP $\beta$  with TLE3 depends on CARM1. Co-expression of WT C/EBP $\beta$  (R) or mutants (R193A, R193L), TLE3, and CARM1 are indicated on the top. WT C/EBP $\beta$ , but not R193A, co-immunoprecipitates with TLE3 in the presence of CARM1, whereas the C/EBP $\beta$ R193L mutation supersedes CARM1 requirement.

(F) RT-PCR of ADIPOQ, CFD, and FABP4 expression (arbitrary units: target gene to internal 36B4 expression control) induced by C/EBP $\beta$  WT, R193A, R193L, or vector control in the absence or presence of TLE3 in NIH 3T3 L1 cells without adipogenic differentiation cocktail (upper panel; n = 3, ANOVA; \*p  $\leq$  0.05, \*\*p  $\leq$  0.01, \*\*\*p  $\leq$  0.001; ns: not significant). Oil red O staining of stably transfected NIH 3T3 L1 cells with C/EBP $\beta$  constructs, vector control and TLE3, as indicated, 3 weeks post-confluency (middle panel, representative images) and protein expression controls (lower panel).

PRMT4/CARM1, the methylation-defective C/EBP $\beta$ R193A mutant failed to bind TLE3, confirming C/EBP $\beta$  CR7 arginine side chain methylation as a prerequisite for binding to TLE3.

Both C/EBP $\beta$  and TLE3 had been described as important regulators in adipogenesis (Villanueva et al., 2013). As shown in Figure 5F, ectopic expression of C/EBP $\beta$  in 3-isobutyl-1-methylxanthine (3T3L1) cells induced partial adipogenic differentiation in the absence of the *in vitro* differentiation cocktail (IBMX, insulin, dexamethasone). Fat cell differentiation was evident by up-regulation of the adipogenic genes ADIPOQ, CFD, and FABP4 (Figure 5F, bar graph panel) and enhanced oil red O staining (below) in local adipogenic nests. Adipogenic gene expression of ADIPOQ and FABP4 was enhanced by the C/EBP $\beta$ R193L mutant, and TLE3 cooperated with C/EBP $\beta$  WT and more strongly with C/EBP $\beta$ R193L, but not with the C/EBP $\beta$ R193A mutant, to activate ADIPOQ, CFD, and FABP4. We conclude that PRISMA may uncover functional C/EBP $\beta$  PTM-regulated protein-protein interactions to adjust the biology of C/EBP $\beta$ .

### Novel Connections between C/EBP $\beta$ , Transcription Elongation, MLL, and NuRD

Of particular interest was the observation that many proteins forming part of the machinery involved in RNAPII pausing and elongation were included in the PRISMA data. Components of the Trithorax MLL/Set1/COMPAS histone H3 lysine 4 (H3K4) methyltransferase complexes (Shilatifard, 2012) were also represented in the dataset, raising the possibility of a connection between C/EBP $\beta$ , enhancer/promoter binding, and regulation of RNAPII processivity. Many components implicated in both processes were found, including the MLL complex components CHD3 and 4 (Mi-2), ASH2, Dpy30, PTIP, and HCF-1; the general transcriptional elongation factor B (TFIIS) and associated elongin A/B/C factors (Aso et al., 1995); the P-TEFb components cyclinK/T1, cdk9, and additional regulatory components including LARP7, HEXIM1, SPT5 (DSIF), and the chromatin adaptor bromodomain factor Brd4 and components of the super elongation complex (SEC), including AF9, PCAF1, and AF4 (AFF1) (Luo et al., 2012). AFF1 is a central SEC scaffold component, and AF9 and ENL are highly similar YEATS domain family members that compete for binding to AFF1. The N-terminal YEATS domain of AF9 and ENL both bind to the PAF complex to connect SEC to RNAPII on chromatin templates. The CDK9/CYCT1 P-TEFb complex is required for rapid transcriptional induction, phosphorylation of the C-terminal domain of RNAPII, and engagement of BRD4, which also interacts with H3K9ac. P-TEFb is also associated with a 7SK snRNA subcomplex that contains the regulatory components LARP7, HEXIM1, and SPT5 (DSIF) and connects to PAFc in the dynamic transcription elongation machinery (He et al., 2011; Luo et al., 2012; Peterlin and Price, 2006). In addition, the histone chaperone FACT complex facilitates passage of the transcription apparatus through chromatin and is thought to restore the chromatin structure and the epigenetic state during transcription, replication, and repair (Hammond et al., 2017; Hondele and Ladurner, 2013; Orphanides et al., 1998).

Immunoprecipitation and immunoblotting were performed to validate several of these novel connections. As shown in Figure 6, multiple MLL, FACT, and SEC components were all co-immunoprecipitated with C/EBP $\beta$ , confirming the predictive capacity of PRISMA. It is also important to note that AFF1, AF9, and



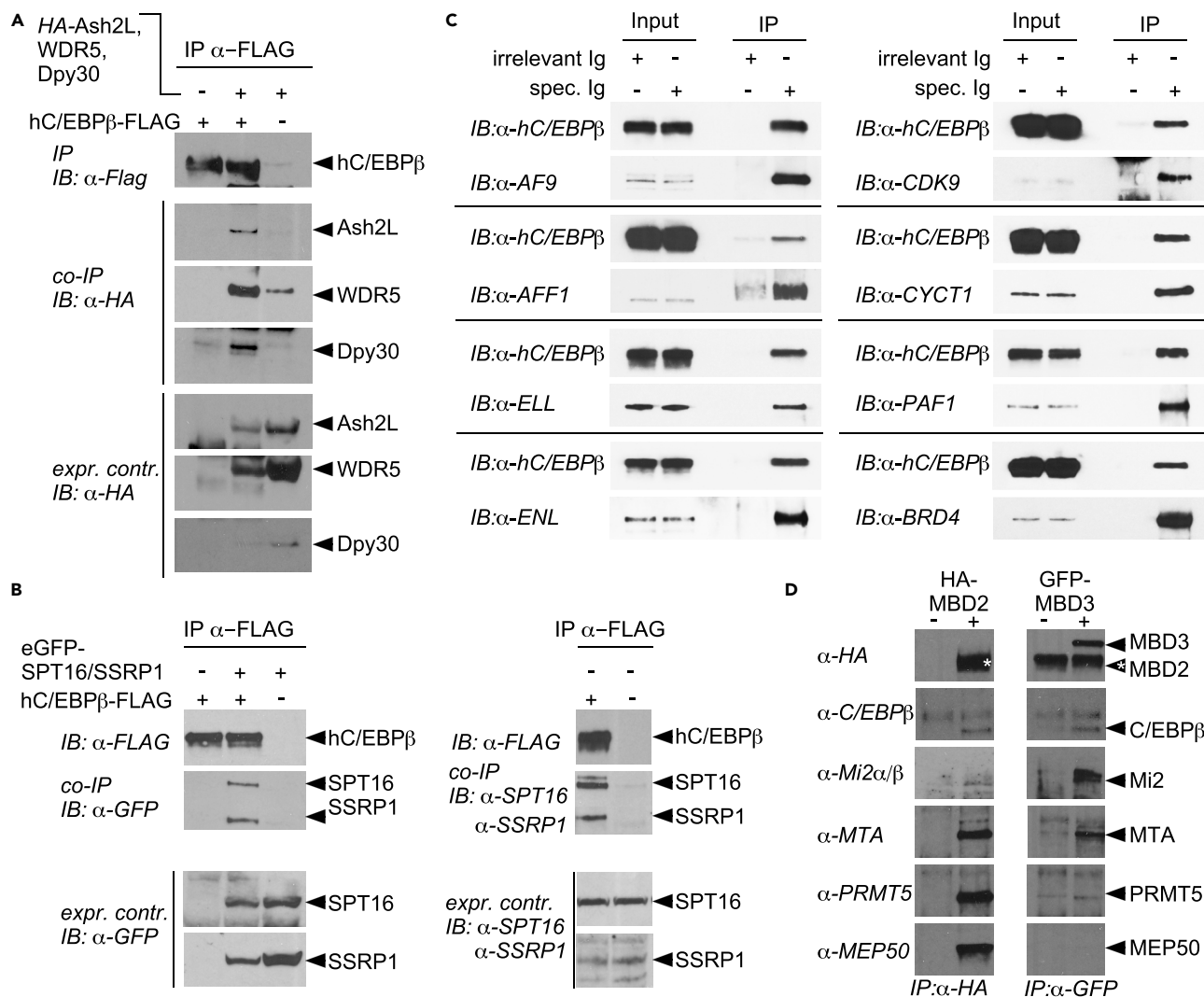


**Figure 6. C/EBPβ-Interacting Multi-protein Complexes in HEK293T Cells**

(A) Co-immunoprecipitation of FLAG-tagged C/EBPβ and the MLL/Ash2/Wdr5 complex.

(B) Left panel: FLAG-tagged C/EBPβ was co-expressed with GFP-tagged Spt16 and Ssrp1. Right panel: Immunoprecipitation of FLAG-tagged C/EBPβ co-precipitates both endogenous FACT complex subunits.

(C) Interaction with the super elongation complex. Immunoprecipitation of human C/EBPβ (C/EBPβ) pulls down the entire super elongation complex.

(D) Interaction with the NuRD complex. The integral subunits of the NuRD complex MBD2 (HA-tagged) and MBD3 (GFP-tagged) were pulled down by immunoprecipitation. Detection by western blot shows that C/EBPβ interacts with both subunits. IB, immunoblotting; IP, immunoprecipitation.

ENL are among the most frequent oncogenic fusion partners with the MLL gene product that transforms early hematopoietic progenitors and causes childhood leukemia by short-circuiting enhancer and promoter activation and transcriptional elongation checkpoint controls (Krivtsov and Armstrong, 2007; Shilatifard, 2012; Slany, 2009; Smith et al., 2011).

The Mi2/NuRD corepressor complex is widely expressed and maintains chromatin in a closed state by ATP-dependent chromatin remodeling and histone tail deacetylation. Some of the NuRD components (CHD3/4(Mi2), HDAC1, RBBP4/7, MTA1,2, GATAD2A/p66α, MBD2, MBD3) identified by PRISMA, SU-DHL1 IP, and other approaches (Steinberg et al., 2012; Siersbaek et al., 2014) are shared with the SIN3A and CoREST repression complexes (Gregoretto et al., 2004), and all were implicated by CORUM analysis (Figures 3 and S3, Table S5). Two major NuRD complexes contain the unique methyl-CpG-binding proteins MBD3 or MBD2, of which the latter may also associate with the WDR77(MEP50)/PRMT5 sub-module (Le Guezennec et al., 2006; Zhang and Yinghua, 2011). Immunoprecipitation of either MBD2 or MBD3 revealed association of C/EBPβ, Mi2, and

MTA with both MBD components, whereas only MBD2 co-precipitated with the WDR77(MEP50)/PRMT5 sub-module, suggesting that C/EBP $\beta$  may associate with both types of NuRD complexes.

## DISCUSSION

In conclusion, the PRISMA technique reveals a comprehensive and PTM-dependent interactome of the disordered C/EBP $\beta$  transcription factor hub and permits the detection of footprints of protein interactions and protein complexes. The results presented in this article suggest that C/EBP $\beta$  is involved at the nexus between enhancer and promoter regulation, in many aspects of pre- and post-transcriptional control, including initiation and pausing control, splicing and exosomal RNA degradation, polyadenylation, and RNA maturation, and in nuclear export. Previously, we described an array peptide screening system (APS) for PTM-dependent protein interactions that relied on fluorophore-based detection of peptide interactions with bacterially expressed human proteins immobilized on macroarrays. Although it is difficult to compare APS with PRISMA because of major differences in peptide choice, peptide length, biochemical conditions, local concentration of interaction partners, signal-to-noise ratio, or complexity of the protein expression library and requirement of a renaturation step, 35 common APS/PRISMA interaction partners, including Brg1/SMARCA4, were found with an N-terminal APS peptide and a comparable section covered in PRISMA that contained CR1 (Pless et al., 2011).

The high local concentration of peptides in matrix spots may limit free diffusion and overcome the dissociation problem of low-affinity interactions (Ruthenburg et al., 2007). These features permit the detection of weak interactions and interactions with rare protein partners. The interaction screen developed herein is augmented by inclusion of amino acids with modified side chains to enable detection of PTM-dependent interactions on a global scale. Together, the interaction footprints and PTM-dependent data may help in the rational design of mutants to further explore the functional C/EBP $\beta$  interactome and aid in the development of pharmacological inhibitors of protein interactions. The PRISMA workflow is applicable to other regulatory proteins and particularly to transcriptional regulators with a high degree of intrinsic disorder, such as Myc- or various Hox proteins. PRISMA may help to discern highly complex and dynamic transcription factor functions that arise through IDR- and PTM-regulated interactions.

PRISMA was developed for analysis of the interactome of proteins with a high degree of intrinsic disorder. Such proteins lack a defined 3D structure, and protein interactions and complex formation are based on SLiMs, PTMs, and intrinsic flexibility. IDRs in conjunction with PTMs may facilitate structural transitions in partner protein exchanges (Wright and Dyson, 2015). Comprehension of the dynamics and context-dependent interactions between structurally flexible SLiMs and various partner proteins is an emerging hallmark of signal transmission and key to understand the regulation of chromatin structure and gene expression (Minde et al., 2017; Tompa et al., 2014; van der Lee et al., 2014; Wright and Dyson, 2015). SLiM interactions often occur with high specificity but low affinity to enable multiple contacts of a dynamic nature, such as occurring during phase separation. Deciphering the functionality of SLiM/MoRF-type protein regions and PTMs in homeostasis and disease can be challenging when using full-length proteins due to functional redundancy and compensatory effects. A variant of PRISMA has meanwhile been employed to detect dysregulated interactions with disease-causing mutations occurring in IDRs (Meyer et al., 2018). PRISMA data presented here thus provide a repository of high-molecular-resolution C/EBP $\beta$  interactions and serve as a basis to explore gene regulatory and PTM-modulated C/EBP $\beta$  functions.

## Limitations of the Study

Protein interactions can be mediated by binding domains or by smaller interaction motifs. One key aspect of the study is the identification of the interactome of IDRs and SLiMs and binding regulation by PTMs. As the PRISMA technique is based on the use of peptides, the detection of interactions is limited to those that are based on structurally variable SLiMs, as binding directly depends on the amino acid sequence properties. The high local concentrations of the peptides on the membrane permit the detection of low-affinity interactors and leave components of their corresponding protein complexes intact under mild washing conditions. For interactions that are based on recognition of three-dimensional structures, however, the method will probably not be applicable.

## METHODS

All methods can be found in the accompanying [Transparent Methods supplemental file](#).

## SUPPLEMENTAL INFORMATION

Supplemental Information can be found online at <https://doi.org/10.1016/j.isci.2019.02.026>.

## ACKNOWLEDGMENTS

We would like to thank Manuel Baesler for generating a web tool (Peptide2Protein) for visualization of PRISMA interactions; Andreas Ladurner, LMU Munich, for FACT expression plasmid constructs; Bernd Lüscher and Juliane Lüscher-Firzlaff, RWTH, Aachen, for MLL complex expression plasmids; and Peter Tontonoz, HHMI, UCLA, for TLE3 constructs. Parts of the work were supported by the CPIL-PEARL grant to G.D. and DFG Grants, LE770/4-2, CRC167B11 to A.L.

## AUTHOR CONTRIBUTIONS

Conceptualization, A.L. and G.D.; Methodology, G.D. and A.L.; Investigation, D.P.H. and G.K.; Validation, E.K.-L., R.W., M.H., M. Knoblich and M. Kirchner; Resources, G.D., A.L., and U.R.; Data curation, G.D., D.P.H., K.B., M. Kirchner, J.W., and A.M.; Writing original draft, A.L.; Writing review and editing, A.L., G.D., E.K.-L., M. Kirchner, K.B.; Visualization, A.L., G.D., A.M., K.B., E.K.-L., and M. Kirchner; Supervision, project administration, and funding acquisition, A.L. (ORCID: 0000-0001-8259-927X) and G.D. (ORCID: 0000-0003-3647-8623).

## DECLARATION OF INTERESTS

The authors declare no competing interest.

Received: August 28, 2017

Revised: January 20, 2019

Accepted: February 23, 2019

Published: March 29, 2019

## REFERENCES

- Agarwal, M., Kumar, P., and Mathew, S.J. (2015). The Groucho/Transducin-like enhancer of split protein family in animal development. *IUBMB Life* 67, 472–481.
- Anastasov, N., Bonzheim, I., Rudelius, M., Klier, M., Dau, T., Angermeier, D., Duyster, J., Pittaluga, S., Fend, F., Raffeld, M., et al. (2010). C/EBPbeta expression in ALK-positive anaplastic large cell lymphomas is required for cell proliferation and is induced by the STAT3 signaling pathway. *Haematologica* 95, 760–767.
- Aso, T., Lane, W.S., Conaway, J.W., and Conaway, R.C. (1995). Elongin (SIII): a multisubunit regulator of elongation by RNA polymerase II. *Science* 269, 1439–1443.
- Bhaumik, P., Davis, J., Tropea, J.E., Cherry, S., Johnson, P.F., and Miller, M. (2014). Structural insights into interactions of C/EBP transcriptional activators with the Taz2 domain of p300. *Acta Crystallogr. Sect. D Biol. Crystallogr.* 70, 1914–1921.
- Conaway, R.C., and Conaway, J.W. (2013). The Mediator complex and transcription elongation. *Biochim. Biophys. Acta* 1829, 69–75.
- D'Haeseleer, P., and Church, G.M. (2004). Estimating and improving protein interaction error rates. *Proc. IEEE Comput. Syst. Inform. Conf.* 216–223.
- Di Stefano, B., Collombet, S., Jakobsen, J.S., Wierer, M., Sardina, J.L., Lackner, A., Stadholders, R., Segura-Morales, C., Francesconi, M., Limone, F., et al. (2016). C/EBPalpha creates elite cells for iPSC reprogramming by upregulating Klf4 and increasing the levels of Lsd1 and Brd4. *Nat. Cell Biol.* 18, 371–381.
- Disfani, F.M., Hsu, W.L., Mizianty, M.J., Oldfield, C.J., Xue, B., Dunker, A.K., Uversky, V.N., and Kurgan, L. (2012). MoRFPred, a computational tool for sequence-based prediction and characterization of short disorder-to-order transitioning binding regions in proteins. *Bioinformatics* 28, i75–83.
- Dunker, A.K., Garner, E., Guillot, S., Romero, P., Albrecht, K., Hart, J., Obradovic, Z., Kissinger, C., and Villafranca, J.E. (1998). Protein disorder and the evolution of molecular recognition: theory, predictions and observations. *Pac. Symp. Biocomput.* 473–484.
- Eaton, E.M., and Sealy, L. (2003). Modification of CCAAT/enhancer-binding protein-beta by the small ubiquitin-like modifier (SUMO) family members, SUMO-2 and SUMO-3. *J. Biol. Chem.* 278, 33416–33421.
- Finn, R.D., Attwood, T.K., Babbitt, P.C., Bateman, A., Bork, P., Bridge, A.J., Chang, H.Y., Dosztanyi, Z., El-Gebali, S., Fraser, M., et al. (2017). InterPro in 2017-beyond protein family and domain annotations. *Nucleic Acids Res.* 45, D190–D199.
- Finn, R.D., Coggill, P., Eberhardt, R.Y., Eddy, S.R., Mistry, J., Mitchell, A.L., Potter, S.C., Punta, M., Qureshi, M., Sangrador-Vegas, A., et al. (2016). The Pfam protein families database: towards a more sustainable future. *Nucleic Acids Res.* 44, D279–D285.
- Gene Ontology, C. (2015). Gene ontology consortium: going forward. *Nucleic Acids Res.* 43, D1049–D1056.
- Gregoret, I.V., Lee, Y.M., and Goodson, H.V. (2004). Molecular evolution of the histone deacetylase family: functional implications of phylogenetic analysis. *J. Mol. Biol.* 16, 338.
- Hammond, C.M., Stromme, C.B., Huang, H., Patel, D.J., and Groth, A. (2017). Histone chaperone networks shaping chromatin function. *Nat. Rev. Mol. Cell Biol.* 18, 141–158.
- He, N., Chan, C.K., Sobhian, B., Chou, S., Xue, Y., Liu, M., Alber, T., Benkirane, M., and Zhou, Q. (2011). Human polymerase-associated factor complex (PAFc) connects the super elongation complex (SEC) to RNA polymerase II on chromatin. *Proc. Natl. Acad. Sci. U S A* 108, E636–E645.
- Hondele, M., and Ladurner, A.G. (2013). Catch me if you can: how the histone chaperone FACT capitalizes on nucleosome breathing. *Nucleus* 4, 443–449.
- Jeronimo, C., and Robert, F. (2017). The mediator complex: at the nexus of RNA polymerase II transcription. *Trends Cell Biol.* 27, 765–783.
- Jundt, F., Raetzl, N., Muller, C., Calkhoven, C.F., Kley, K., Mathas, S., Lietz, A., Leutz, A., and Dorken, B. (2005). A rapamycin derivative (everolimus) controls proliferation through down-regulation of truncated CCAAT enhancer binding protein {beta} and NF- $\kappa$ B activity in

- Hodgkin and anaplastic large cell lymphomas. *Blood* 106, 1801–1807.
- Kajimura, S., Seale, P., Kubota, K., Lunsford, E., Frangioni, J.V., Gygi, S.P., and Spiegelman, B.M. (2009). Initiation of myoblast to brown fat switch by a PRDM16-C/EBP-beta transcriptional complex. *Nature* 460, 1154–1158.
- Kovacs, K.A., Steinmann, M., Magistretti, P.J., Halfon, O., and Cardinaux, J.R. (2003). CCAAT/enhancer-binding protein family members recruit the coactivator CREB-binding protein and trigger its phosphorylation. *J. Biol. Chem.* 278, 36959–36965.
- Kowenz-Leutz, E., and Leutz, A. (1999). A C/EBP beta isoform recruits the SWI/SNF complex to activate myeloid genes. *Mol. Cell* 4, 735–743.
- Kowenz-Leutz, E., Pless, O., Dittmar, G., Knoblich, M., and Leutz, A. (2010). Crosstalk between C/EBPbeta phosphorylation, arginine methylation, and SWI/SNF/Mediator implies an indexing transcription factor code. *EMBO J.* 29, 1105–1115.
- Kowenz-Leutz, E., Twamley, G., Ansieau, S., and Leutz, A. (1994). Novel mechanism of C/EBP beta (NF-M) transcriptional control: activation through derepression. *Genes Dev.* 8, 2781–2791.
- Krivtsov, A.V., and Armstrong, S.A. (2007). MLL translocations, histone modifications and leukaemia stem-cell development. *Nat. Rev. Cancer* 7, 823–833.
- Le Guezennec, X., Vermeulen, M., Brinkman, A.B., Hoesjmakers, W.A., Cohen, A., Lasonder, E., and Stunnenberg, H.G. (2006). MBD2/NuRD and MBD3/NuRD, two distinct complexes with different biochemical and functional properties. *Mol. Cell. Biol.* 26, 843–851.
- Lee, S., Miller, M., Shuman, J.D., and Johnson, P.F. (2010a). CCAAT/Enhancer-binding protein beta DNA binding is auto-inhibited by multiple elements that also mediate association with p300/CREB-binding protein (CBP). *J. Biol. Chem.* 285, 21399–21410.
- Lee, S., Shuman, J.D., Guszczynski, T., Sakchaisri, K., Sebastian, T., Copeland, T.D., Miller, M., Cohen, M.S., Taunton, J., Smart, R.C., et al. (2010b). RSK-mediated phosphorylation in the C/EBP{beta} leucine zipper regulates DNA binding, dimerization, and growth arrest activity. *Mol. Cell. Biol.* 30, 2621–2635.
- Leutz, A., Pless, O., Lappe, M., Dittmar, G., and Kowenz-Leutz, E. (2011). Crosstalk between phosphorylation and multi-site arginine/lysine methylation in C/EBPs. *Transcription* 2, 3–8.
- Lichtinger, M., Ingram, R., Hannah, R., Müller, D., Clarke, D., Assi, S.A., Lie-A-Ling, M., Noailles, L., Vijayabaskar, M.S., Wu, M., et al. (2012). RUNX1 reshapes the epigenetic landscape at the onset of haematopoiesis. *EMBO J.* 31, 4318–4333.
- Luo, Z., Lin, C., and Shilatifard, A. (2012). The super elongation complex (SEC) family in transcriptional control. *Nat. Rev. Mol. Cell. Biol.* 13, 543–547.
- Lynch, V.J., May, G., and Wagner, G.P. (2011). Regulatory evolution through divergence of a phosphoswitch in the transcription factor CEBPB. *Nature* 480, 383–386.
- Meszaros, B., Simon, I., and Dosztanyi, Z. (2009). Prediction of protein binding regions in disordered proteins. *PLoS Comput. Biol.* 5, e1000376.
- Meyer, K., Kirchner, M., Uyar, B., Cheng, J.Y., Russo, G., Hernandez-Miranda, L.R., Szymborska, A., Zauber, H., Rudolph, I.M., Willnow, T.E., et al. (2018). Mutations in disordered regions can cause disease by creating dileucine motifs. *Cell* 175, 239–253.e17.
- Miller, M. (2006). Phospho-dependent protein recognition motifs contained in C/EBP family of transcription factors: in silico studies. *Cell Cycle* 5, 2501–2508.
- Minde, D.P., Dunker, A.K., and Lilley, K.S. (2017). Time, space, and disorder in the expanding proteome universe. *Proteomics* 17, <https://doi.org/10.1002/psmic.201600399>.
- Mo, X., Kowenz-Leutz, E., Xu, H., and Leutz, A. (2004). Ras induces mediator complex exchange on C/EBP beta. *Mol. Cell* 13, 241–250.
- Mohan, A., Oldfield, C.J., Radivojac, P., Vacic, V., Cortese, M.S., Dunker, A.K., and Uversky, V.N. (2006). Analysis of molecular recognition features (MoRFs). *J. Mol. Biol.* 362, 1043–1059.
- Muller, C., Kowenz-Leutz, E., Grieser-Ade, S., Graf, T., and Leutz, A. (1995). NF-M (chicken C/EBP beta) induces eosinophilic differentiation and apoptosis in a hematopoietic progenitor cell line. *EMBO J.* 14, 6127–6135.
- Muller-McNicol, M., and Neugebauer, K.M. (2013). How cells get the message: dynamic assembly and function of mRNA-protein complexes. *Nat. Rev. Genet.* 14, 275–287.
- Nerlov, C. (2008). C/EBPs: recipients of extracellular signals through proteome modulation. *Curr. Opin. Cell Biol.* 20, 180–185.
- Ness, S.A., Kowenz-Leutz, E., Casini, T., Graf, T., and Leutz, A. (1993). Myb and NF-M: combinatorial activators of myeloid genes in heterologous cell types. *Genes Dev.* 7, 749–759.
- Orphanides, G., LeRoy, G., Chang, C.H., Luse, D.S., and Reinberg, D. (1998). FACT, a factor that facilitates transcript elongation through nucleosomes. *Cell* 92, 105–116.
- Peterlin, B.M., and Price, D.H. (2006). Controlling the elongation phase of transcription with P-TEFb. *Mol. Cell* 23, 297–305.
- Pless, O., Kowenz-Leutz, E., Dittmar, G., and Leutz, A. (2011). A differential proteome screening system for post-translational modification-dependent transcription factor interactions. *Nat. Protoc.* 6, 359–364.
- Pless, O., Kowenz-Leutz, E., Knoblich, M., Lausen, J., Beyermann, M., Walsh, M.J., and Leutz, A. (2008). G9a-mediated lysine methylation alters the function of CCAAT/enhancer-binding protein-beta. *J. Biol. Chem.* 283, 26357–26363.
- Reimand, J., Arak, T., Adler, P., Kolberg, L., Reisberg, S., Peterson, H., and Vilo, J. (2016). g:Profiler—a web server for functional interpretation of gene lists (2016 update). *Nucleic Acids Res.* 44, W83–W89.
- Rodier, F., and Campisi, J. (2011). Four faces of cellular senescence. *J. Cell Biol.* 192, 547–556.
- Ruepp, A., Waegele, B., Lechner, M., Brauner, B., Dunger-Kaltenbach, I., Fobo, G., Frishman, G., Montrone, C., and Mewes, H.W. (2010). CORUM: the comprehensive resource of mammalian protein complexes—2009. *Nucleic Acids Res.* 38, D497–D501.
- Ruthenburg, A.J., Allis, C.D., and Wysocka, J. (2007). Methylation of lysine 4 on histone H3: intricacy of writing and reading a single epigenetic mark. *Mol. Cell* 25, 15–30.
- Schwanhauser, B., Busse, D., Li, N., Dittmar, G., Schuchhardt, J., Wolf, J., Chen, W., and Selbach, M. (2011). Global quantification of mammalian gene expression control. *Nature* 473, 337–342.
- Schwartz, C., Beck, K., Mink, S., Schmolke, M., Budde, B., Wenning, D., and Klempnauer, K.H. (2003). Recruitment of p300 by C/EBPbeta triggers phosphorylation of p300 and modulates coactivator activity. *EMBO J.* 22, 882–892.
- Sebastian, T., Malik, R., Thomas, S., Sage, J., and Johnson, P.F. (2005). C/EBPbeta cooperates with RB: E2F to implement Ras(V12)-induced cellular senescence. *EMBO J.* 24, 3301–3312.
- Shilatifard, A. (2012). The COMPASS family of histone H3K4 methylases: mechanisms of regulation in development and disease pathogenesis. *Annu. Rev. Biochem.* 81, 65–95.
- Siersbaek, R., Nielsen, R., John, S., Sung, M.H., Baek, S., Loft, A., Hager, G.L., and Mandrup, S. (2011). Extensive chromatin remodelling and establishment of transcription factor ‘hotspots’ during early adipogenesis. *EMBO J.* 30, 1459–1472.
- Siersbaek, R., Rabiee, A., Nielsen, R., Sidoli, S., Traynor, S., Loft, A., La Cour Poulsen, L., Rogowska-Wrzemesinska, A., Jensen, O.N., and Mandrup, S. (2014). Transcription factor cooperativity in early adipogenic hotspots and super-enhancers. *Cell Rep.* 7, 1443–1455.
- Slany, R.K. (2009). The molecular biology of mixed lineage leukemia. *Haematologica* 94, 984–993.
- Smith, E., Lin, C., and Shilatifard, A. (2011). The super elongation complex (SEC) and MLL in development and disease. *Genes Dev.* 25, 661–672.
- Smits, A.H., Jansen, P.W., Poser, I., Hyman, A.A., and Vermeulen, M. (2013). Stoichiometry of chromatin-associated protein complexes revealed by label-free quantitative mass spectrometry-based proteomics. *Nucleic Acids Res.* 41, e28.
- Steinberg, X.P., Hepp, M.I., Fernandez Garcia, Y., Suganuma, T., Swanson, S.K., Washburn, M., Workman, J.L., and Gutierrez, J.L. (2012). Human CCAAT/enhancer-binding protein beta interacts with chromatin remodeling complexes of the imitation switch subfamily. *Biochemistry* 51, 952–962.
- Sterneck, E., Tassarollo, L., and Johnson, P.F. (1997). An essential role for C/EBPbeta in female reproduction. *Genes Dev.* 11, 2153–2162.
- Stoilova, B., Kowenz-Leutz, E., Scheller, M., and Leutz, A. (2013). Lymphoid to myeloid cell trans-differentiation is determined by C/EBPbeta

structure and post-translational modifications. *PLoS One* 8, e65169.

Tompa, P., Davey, N.E., Gibson, T.J., and Babu, M.M. (2014). A million peptide motifs for the molecular biologist. *Mol. Cell* 55, 161–169.

Tsukada, J., Yoshida, Y., Kominato, Y., and Auron, P.E. (2011). The CCAAT/enhancer (C/EBP) family of basic-leucine zipper (bZIP) transcription factors is a multifaceted highly-regulated system for gene regulation. *Cytokine* 54, 6–19.

Tyanova, S., Temu, T., Sinitcyn, P., Carlson, A., Hein, M.Y., Geiger, T., Mann, M., and Cox, J. (2016). The Perseus computational platform for comprehensive analysis of (prote)omics data. *Nat. Methods* 13, 731–740.

van der Lee, R., Buljan, M., Lang, B., Weatheritt, R.J., Daughdrill, G.W., Dunker, A.K., Fuxreiter, M., Gough, J., Gsponer, J., Jones, D.T., et al. (2014).

Classification of intrinsically disordered regions and proteins. *Chem. Rev.* 114, 6589–6631.

Villanueva, C.J., Vergnes, L., Wang, J., Drew, B.G., Hong, C., Tu, Y., Hu, Y., Peng, X., Xu, F., Saez, E., et al. (2013). Adipose subtype-selective recruitment of TLE3 or Prdm16 by PPARgamma specifies lipid storage versus thermogenic gene programs. *Cell Metab.* 17, 423–435.

Weake, V.M., and Workman, J.L. (2012). SAGA function in tissue-specific gene expression. *Trends Cell Biol.* 22, 177–184.

Wethmar, K., Smink, J.J., and Leutz, A. (2010). Upstream open reading frames: molecular switches in (patho)physiology. *BioEssays* 32, 885–893.

Wickramasinghe, V.O., and Laskey, R.A. (2015). Control of mammalian gene expression by selective mRNA export. *Nat. Rev. Mol. Cell Biol.* 16, 431–442.

Williams, S.C., Baer, M., Dillner, A.J., and Johnson, P.F. (1995). CRP2 (C/EBP beta) contains a bipartite regulatory domain that controls transcriptional activation, DNA binding and cell specificity. *EMBO J.* 14, 3170–3183.

Wright, P.E., and Dyson, H.J. (1999). Intrinsically unstructured proteins: re-assessing the protein structure-function paradigm. *J. Mol. Biol.* 293, 321–331.

Wright, P.E., and Dyson, H.J. (2015). Intrinsically disordered proteins in cellular signalling and regulation. *Nat. Rev. Mol. Cell Biol.* 16, 18–29.

Xie, H., Ye, M., Feng, R., and Graf, T. (2004). Stepwise reprogramming of B cells into macrophages. *Cell* 117, 663–676.

Zhang, and Yinghua, L. (2011). The expanding Mi-2/NuRD complexes: a schematic glance. *Proteomics Insights* 3, 79–109.

## **Supplemental Information**

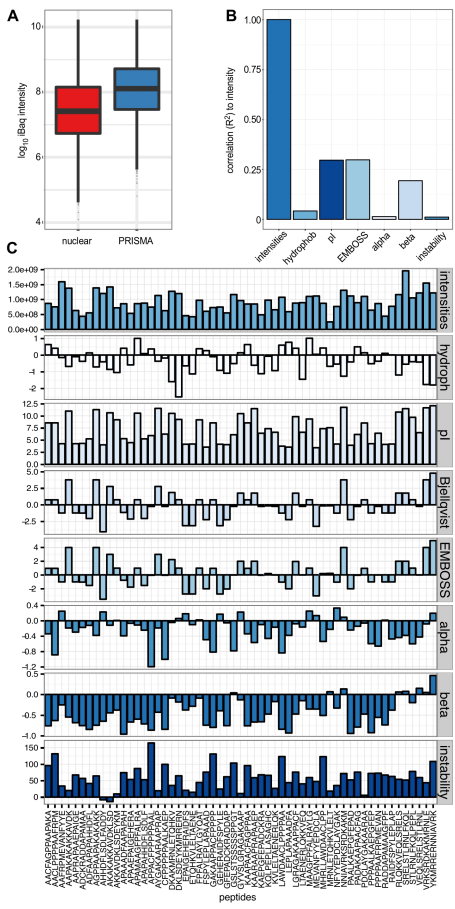
### **PRISMA: Protein Interaction Screen on Peptide Matrix**

#### **Reveals Interaction Footprints and Modifications-**

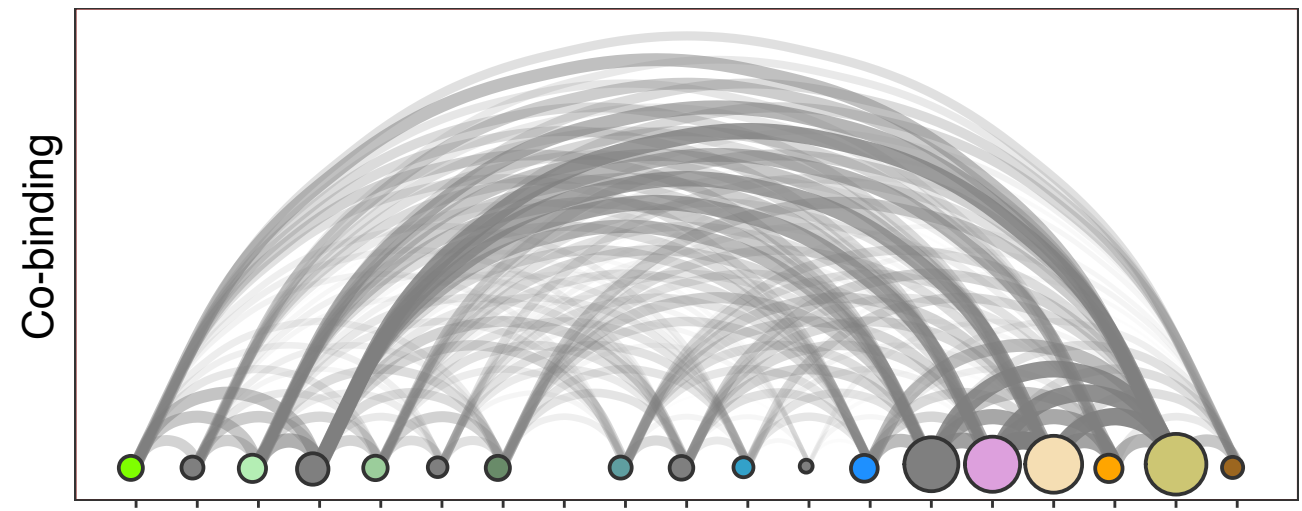
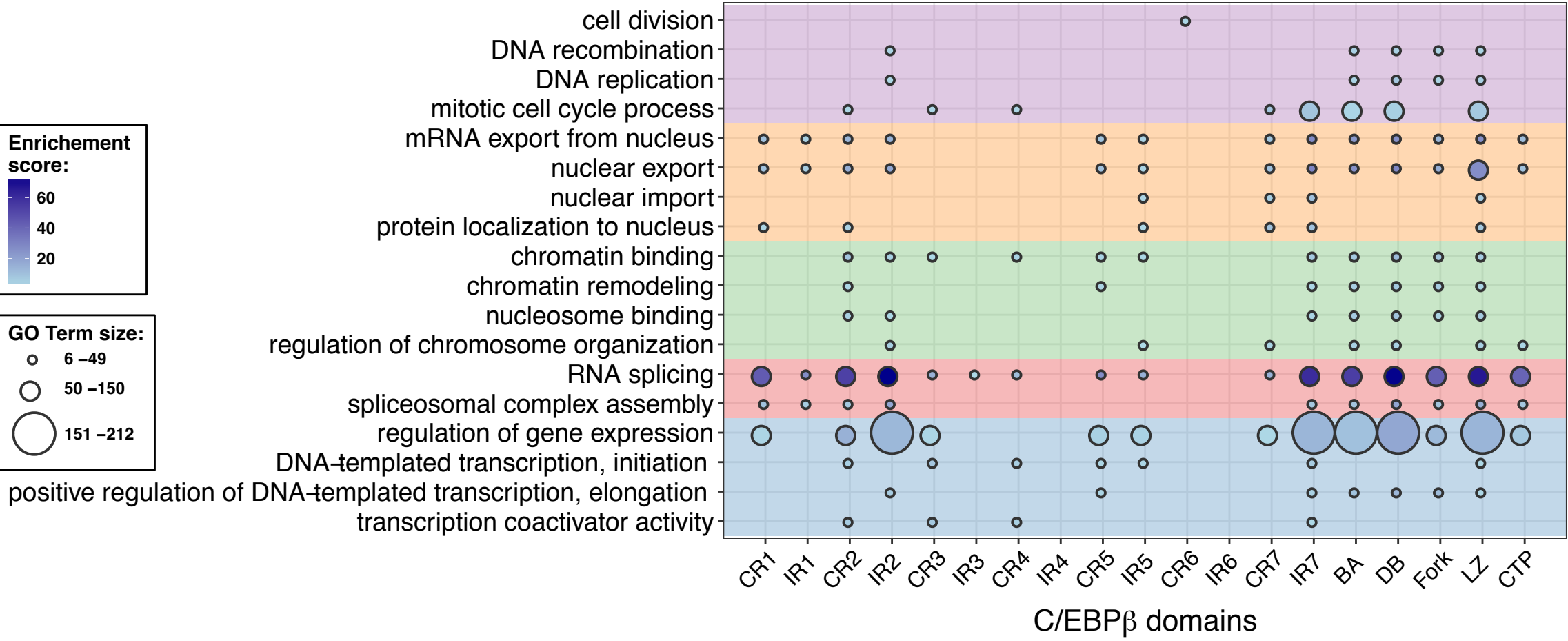
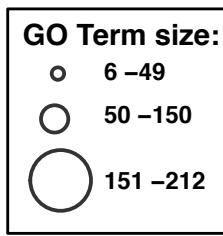
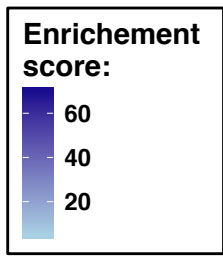
#### **Dependent Interactome of Intrinsically Disordered C/EBP $\beta$**

**Gunnar Dittmar, Daniel Perez Hernandez, Elisabeth Kowenz-Leutz, Marielise Kirchner, Günther Kahlert, Radoslaw Wesolowski, Katharina Baum, Maria Knoblich, Maria Hofstätter, Arnaud Muller, Jana Wolf, Ulf Reimer, and Achim Leutz**





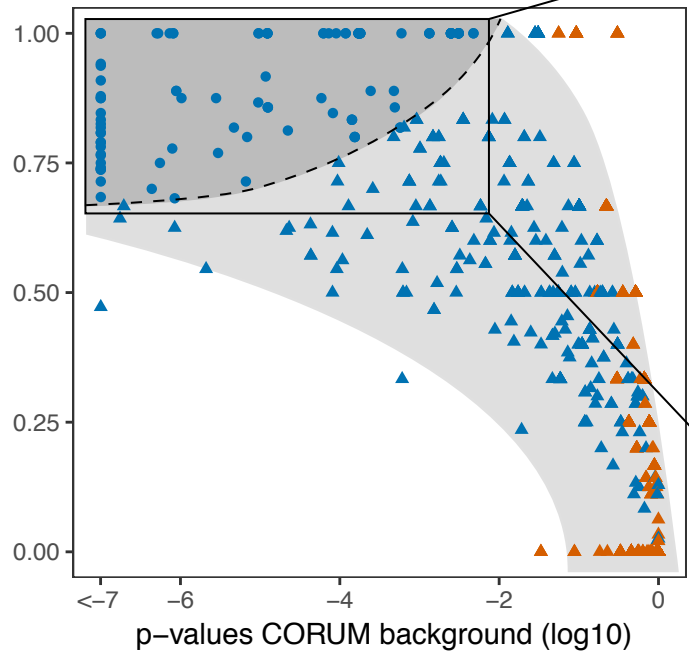
**Supplemental Figure 1: Comparison of enrichment by PRISMA and physico-chemical properties of PRISMA peptides. Related to Figures 1 and 2.** **A.** Distribution of the copy number. Estimations based on the iBaq quantification for the PRISMA screen and the nuclear extracts. Both, nuclear extracts and PRISMA binders are in the same copy number range. **B.** Correlation of the accumulated intensity of the PRISMA binders to different peptide properties. **C.** Binding of proteins in the PRISMA screen in comparison to various calculated peptide properties. The top panel shows the accumulated binding intensity of the PRISMA binders, while the other panels show the different calculated peptide properties for the peptides listed below.

**A****B**

**Supplemental Figure 2: Internal C/EBP $\beta$  connections and GO term distribution.**

**Related to Figure 2. A.** Co-binding of interaction partners to different C/EBP $\beta$  regions. The number of interaction partners was calculated that bind to two different regions, as indicated on the abscissa. Dot sizes represent the number of binding partners in the C/EBP $\beta$  regions, while the width of the arcs represent the number of interaction partners found in the connected regions. **B.** Enrichment analysis of GO-terms for binding partners in the different regions of C/EBP $\beta$ . GO-terms were selected for DNA related processes (pink), nuclear import/export (orange), chromatin (green), RNA splicing (red) and transcription (blue).

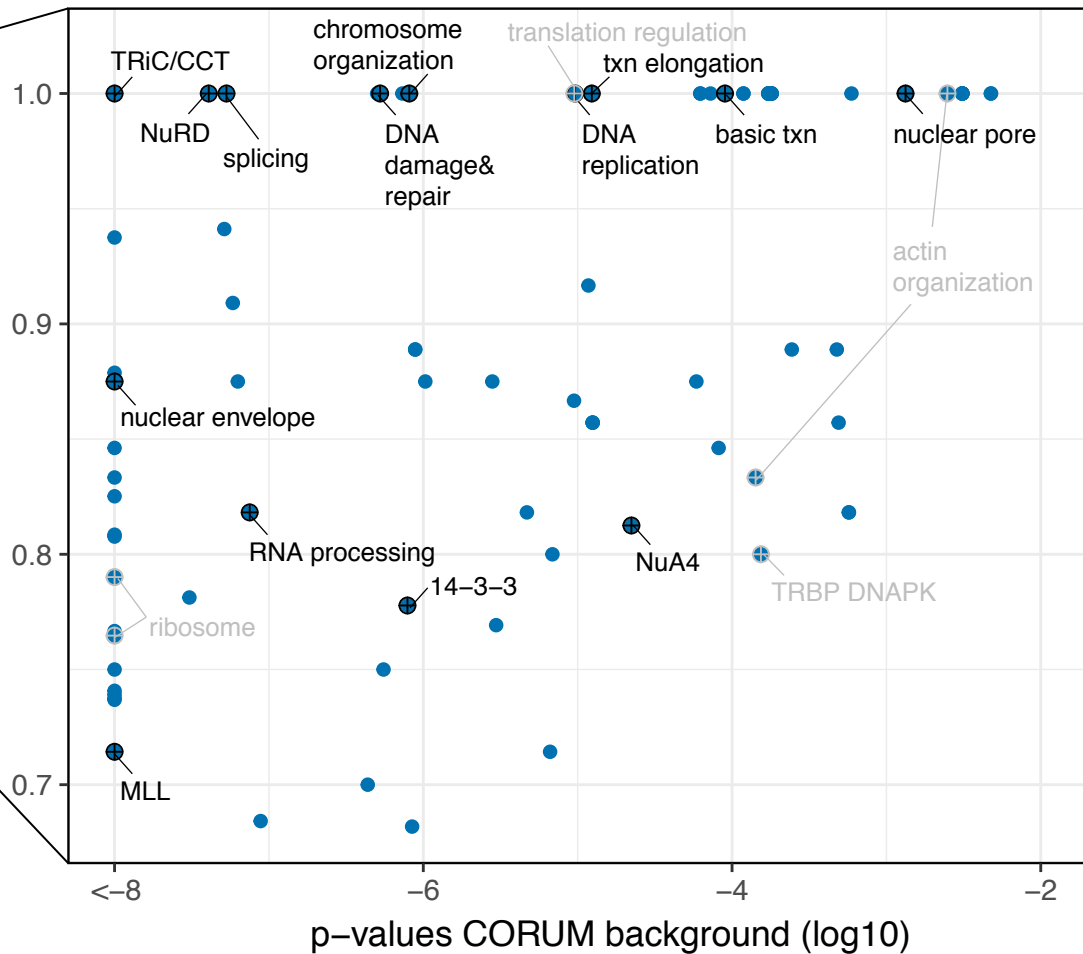
complex coverage by PRISMA



- ▲ complex rank  $> 104$
- complex rank  $\leq 104$

- $> 0$  PRISMA hits and  $> 2$  hits in PRISMA and SU-DHL1
- 0 PRISMA hits or  $< 3$  hits in PRISMA and SU-DHL1

complex coverage by PRISMA



**Supplemental Figure 3: Potential C/EBP $\beta$  interacting protein complexes. Related to Figure 3.** Complex coverage and p-values for each of the 1432 complexes as used for the ranking of CORUM complexes (**Additional Information below**). Each dot corresponds to one complex. Red symbols show complexes which have less than three protein hits in PRISMA and SU-DHL1 data sets. Circles represent complexes ranking within the upper quartile (dark grey) (104 complexes, dashed line between upper quartile and lower ranks), triangles encode lower ranking complexes. The 104 highest ranking complexes are shown in the close-up on the right. Highest ranking complexes for each of the 14 categories from Fig. 4B are indicated in black; other complexes which are not included in Fig. 4A, in grey.





**Supplemental Figure 4: PTM-dependent binding across C/EBP $\beta$ . Related to Figure 5.**

The positions of the PTM-modified peptides are shown on the schematic presentation of the primary C/EBP $\beta$  sequence on top. For each peptide, the relative binding to the PTM-modified peptides was calculated in relation to the unmodified peptide. Heatmaps display the relative binding of the proteins on the y-axis in relation to different PTM-carrying peptides, indicated below the heat maps. Red indicates enhanced binding and blue shows reduced binding. Note that the Figure has infinite zoom function for detailed inspection of data.

## **Transparent Methods**

### **Peptide matrix synthesis**

Peptides were synthesized using the automated high-throughput SPOT-synthesis method (Kramer and Schneider-Mergener, 1998). Briefly, Whatman 50 cellulose membranes (Whatman, UK) were functionalized by coupling of Fmoc-protected  $\beta$ -alanine in defined spots. Subsequently, peptides were synthesized stepwise using standard Fmoc-chemistry. After each coupling step before Fmoc-deprotection, peptides that failed coupling of building blocks were acetylated to avoid false sequences.

### **Interaction screen**

The peptide matrix membrane was blocked with yeast tRNA (1 mg/ml; Invitrogen, Karlsruhe, Germany) in binding buffer (20 mM HEPES pH 7.9, Merck, Germany, 0.2 mM EDTA, Merck, Germany, 100 mM KCl Merck, Germany, 20% glycerol, Merck, Germany, 0.5 mM DTT, Merck, Germany) to minimize unspecific protein binding. The membrane was then incubated with HeLa cell nuclear extract (5 mg/ml; Calbiotech S.A, Germany) in binding buffer supplemented with 0.5 mM PMSF (Merck, Germany) for 30 min, then briefly washed with binding buffer. Peptide spots were individually excised and bound proteins converted to peptides using a two-step digest with endopeptidase LysC (Wako, Japan) followed by sequencing-grade trypsin (Promega, Germany) using a robotic setup (Kanashova et al., 2015). Peptide extracts were purified and stored on stage tips (Rappsilber et al., 2007). Two replicates were measured for each peptide spot.

### **Mass spectrometry measurement for PRISMA**

Peptides were cleaned up using a stage-tip micro column (Rappsilber et al., 2007) and resuspended in water with 0.1% formic acid (Merck, Germany). Peptides were separated on a 15cm reverse-phase column (packed in-house, 75  $\mu$ m inner diameter, 3  $\mu$ m C<sub>18</sub>-Reprosil beads; Dr Maisch GmbH, Ammerbruch, Germany) using a gradient to 40% acetonitrile (Merck,

Germany) developed over 1 h 5 min. Separated peptides were ionized on a Proxeon ion source and directly sprayed into the online-coupled VELOS-OrbiTRAP mass spectrometer (Thermo scientific). MS<sup>1</sup> spectra were recorded with a mass resolution of 60,000 in the orbitrap part of the machine. MS<sup>2</sup> spectra were recorded in the VELOS. The ten most intense ions with a charge state greater than 1 were selected (target value = 500; monoisotopic precursor selection enabled) and fragmented in the linear quadrupole trap using CID (collision induced dissociation, 35% normalized collision energy). Dynamic exclusion for selected precursor ions was 60 s. Recorded spectra were analyzed using MaxQuant software package version 1.2.2.5 (Cox and Mann, 2008) and the human IPI database (version 3.3.72), allowing for 2 missed cleavages. Fixed modifications were set to cysteine carbamylation, and variable modifications were set to methionine oxidation, as well as N-terminal protein acetylation. Each replicate was analyzed separately with the label-free option activated for data quantification (Cox et al., 2011).

### **Analysis of nuclear cell extracts**

Nuclear cell extracts were supplemented with the USP2 standard (Merck, Germany) and digested as described above on an automated digestion setup (Kanashova et al., 2015). Peptides were fractionated by RP-HPLC with Proxeon nLC2 and further analyzed by a QExactive mass spectrometer (Thermo Scientific). The mass spectrometer was operated in a data-dependent acquisition mode with dynamic exclusion enabled (30 s). MS<sup>1</sup> (mass range 300-1700 Th) was acquired at a resolution of 70,000 with the ten most abundant multiply charged ( $z \geq 2$ ), ions selected with a 2 Th isolation window for HCD (Higher-energy collisional dissociation) fragmentation. MS<sup>2</sup> scans were acquired at a resolution of 17,500 and injection time of 60 ms.

## Full-length C/EBP $\beta$ interactome analysis by AP-MS mass spectrometry

Eluates from control immunoglobulins (IgG) and anti-C/EBP $\beta$  pull-downs (four replicates each) were ethanol precipitated and protein pellets were solubilised in urea buffer (6 M urea, 2 M thiourea, 20 mM HEPES pH 8), reduced for 30 min at RT in 10 mM DTT, followed by alkylation with 55 mM chloroacetamide (Merck, Germany) for 20 min in the dark at RT. The endopeptidase LysC (Wako, Japan) was added at a protein:enzyme ratio of 50:1 and incubated for 4h at RT. After dilution of the sample with 4 $\times$  digestion buffer (50 mM ammonium bicarbonate pH 8), sequence-grade modified trypsin (Promega, Darmstadt, Germany) was added (protein:enzyme ratio = 100:1) and digested overnight. Trypsin and LysC activity was quenched by acidification with trifluoroacetic acid (TFA) added to pH ~2. Afterwards, peptides were extracted and desalted using the standard StageTip protocol (Rappsilber et al, 2003). Peptide mixtures were separated by reverse-phase chromatography using an Eksigent NanoLC 400 system (Sciex, Darmstadt, Germany) on in-house-manufactured 20 cm fritless silica microcolumns with an inner diameter of 75  $\mu$ m. Columns were packed with ReproSil-Pur C18-AQ 3  $\mu$ m resin (Dr Maisch GmbH). Peptides were separated using an 8–60% acetonitrile gradient (ran over 224 min) at a nanoflow rate of 250 nl/min. Eluting peptides were directly ionised by electrospray ionization and analyzed on a Thermo Orbitrap Fusion instrument (Q-OT-qIT, Thermo). Survey scans of peptide precursors from 300 to 1500  $m/z$  were performed at 120 K resolution with a  $2 \times 10^5$  ion count target. Tandem MS was performed by isolation at 1.6  $m/z$  with the quadrupole, HCD fragmentation with a normalized collision energy of 30, and rapid scan MS analysis in the ion trap. The MS<sup>2</sup> ion count target was set to  $2 \times 10^3$  and the max injection time was 300 ms. Only precursors with a charge state of 2–7 were sampled for MS<sup>2</sup>. The dynamic exclusion duration was set to 60 s with a 10 ppm tolerance around the selected precursor and its isotopes. The instrument was run in top speed mode with 3 s cycles, meaning the instrument could continuously perform MS<sup>2</sup> events until the list of non-excluded precursors diminished to zero or 3 s. Data were analyzed by MaxQuant software version 1.5.1.2. The internal Andromeda search engine was used to search MS<sup>2</sup> spectra against a decoy human UniProt database (HUMAN.2014-10) containing forward and reverse sequences. The search

included variable modifications of methionine oxidation and N-terminal acetylation, deamidation (N and Q) and fixed modification of carbamidomethyl cysteine. The minimal peptide length was set to seven amino acids, and a maximum of two missed cleavages were allowed. The FDR was set to 0.01 for peptide and protein identifications. Unique and razor peptides with a minimum ratio count of 1 were considered for quantification. Retention times were recalibrated based on the built-in nonlinear time-rescaling algorithm. MS<sup>2</sup> identifications were transferred between runs with the 'Match between runs' option, in which the maximal retention time window was set to 0.7 min. Statistical analysis was performed using Perseus version 1.5.2.4. C/EBP $\beta$  pull-down and control samples were defined as groups and proteins and filtered by intensity value using a 'minimum value of 3 per group' as the threshold. After log<sub>2</sub> transformation, missing values were imputed with random numbers from a normal distribution with a mean and standard deviation chosen to best simulate low abundance values below the noise level (width = 0.3; shift = 1.8). Significantly enriched proteins were determined using a volcano plot-based strategy, combining standard two-sample t-test *p*-values with ratio information. Significance corresponding to an FDR of 5% was determined by a permutation-based method (Tusher et al., 2001). Equal sample load was confirmed by calculating the ratio of antibody intensities (mean log<sub>2</sub> ratio = 0.1575).

### **Identification of C/EBP $\beta$ PTM sites by mass spectrometry**

Eluates of anti-C/EBP $\beta$  pull-downs were ethanol precipitated and protein pellets were processed as described above for the interactome analyses. Peptides were analyzed on a Thermo Orbitrap Fusion instrument (Q-OT-qIT, Thermo). Sequential survey scans of peptide precursors covering different mass ranges (300–600, 550–850, 800–1100, 1050–1700 *m/z*) were performed at 120 K resolution with a  $2 \times 10^5$  ion count target on the three most abundant precursor ions. Tandem MS was performed by isolation at 1.6 *m/z* with the quadrupole, HCD fragmentation with a normalized collision energy of 30, and rapid scan MS analysis in the ion trap. The MS<sup>2</sup> ion count target was set to  $1 \times 10^4$  and the max injection time was 500 ms. Only precursors with a charge state of 2–7 were sampled for MS<sup>2</sup>. The dynamic exclusion duration

was set to 60 s with a 10 ppm tolerance around the selected precursor and its isotopes. Data were analyzed by MaxQuant software version 1.5.1.2 as described above for interactome analysis with some modifications; the search included variable modifications of methionine oxidation and N-terminal acetylation, deamidation (N and Q), phosphorylation (S, T and Y), acetylation (K), methylation (K and R), dimethylation (K and R), trimethylation (K) and citrullination (R). Modification of carbamidomethyl cysteine was set as a fixed modification. The minimal peptide length was set to seven amino acids, and a maximum of four missed cleavages were allowed. The FDR was set to 0.01 for site identifications. To filter for confidently identified peptides, the MaxQuant score was set to a minimum of 40. Identified PTM sites were classified according to their localization probability (Class I >0.75, Class II >0.5, Class 3 >0.25). In order to distinguish citrullination from deamidation, a modification resulting in a similar mass shift of the precursor, both modifications were included during MaxQuant data analyses as variable modifications, and at least one missed cleavage was required for citrullination site identification. When arginine and lysine are acetylated or methylated, trypsin often fails to cleave at that site, resulting in miss-cleaved peptides. Therefore, only the PTM sites, which were identified within the peptide, but not C-terminally localized, were considered as confidently identified.

### **Combining the two datasets and data filtering**

The two datasets of the PRISMA measurement were analyzed in two batches due to restrictions of the MaxQuant software package. The two separate datasets were then integrated by calculating the average intensity value where two values were available, or by taking the single measured value if only one intensity measurement was available to prevent bias against single identifications. Single value intensities were annotated as lower confidence quantifications. Each of the data rows of the combined dataset, corresponding to intensity values of one protein over all 203 peptides, was first filtered according to the outlier criterion  $I_n = 0$  if  $I_n \leq P90$ , where  $I_n$  is the intensity at peptide  $n$ , and  $P90$  is the 90th percentile of the intensity value distribution of the protein, followed by normalization against the intensity of the



highest value in each row using  $\frac{I_n}{\max_k(I_k)} = I_n$ , where  $I_n$  is the intensity at peptide  $n$ . This was followed by an additional filtering step where all proteins were removed that did not show a consecutive binding pattern according to finding at least one intensity  $I_n$  with  $I_n > 0$  and  $I_{n+1} > 0$  with  $I_n$  as the intensity at peptide  $n$  and only considering peptides without any PTM.

### **Construction of CORUM networks**

For each complex identified in the CORUM database, the corresponding UniProt identifier was extracted and translated to an ensemblp identifier using the bioDBnet conversion tool (Mudunuri et al., 2009). For each of the ensemblp identifiers, interactions were extracted from the STRING resource (Szklarczyk et al., 2015). The interaction network was constructed using the igraph software package (Csardi G, 2006) and colored based on the source of the interaction from the different datasets.

### **Relative binding to PTM-modified peptides**

For each peptide and its PTM derivatives, the relative binding was calculated. For each protein and modified peptide, the intensity value of the unmodified form of the peptide was subtracted. The resulting values were separated into five fractions and clustered according to their Euclidian distance.

### **Calculation of peptide properties**

For calculation of peptide properties, the R peptides package was used, and properties were calculated and plotted using the ggplot2 packages (Wickham, 2009).

### **Use of the DAVID package**

A total of 1375 identifiers were examined using the Generic Gene Ontology Term Finder (GGOTF, Princeton University, Lewis-Sigler Institute for Integrative Genomics) to assess ontology aspects, functions, and components.

### **Immunoprecipitation of endogenous C/EBP $\beta$ for mass spectrometry**

Immunoprecipitation of C/EBP $\beta$  from  $4 \times 10^8$  SU-DHL1 cells (anaplastic large cell lymphoma, DSMZ, ACC 356) was performed after washing twice with phosphate-buffered saline (PBS) and resuspension in lysis buffer (20 mM HEPES pH 7.5, 150 mM NaCl, 5 mM MgCl<sub>2</sub>, 1 mM EDTA pH 8), 1  $\mu$ M ZnCl<sub>2</sub> (Merck, Germany), 0.1% NP40 (Sigma, Germany), 2 mM dithiothreitol (DTT), 2 mM PEFAbloc (Böhringer, Mannheim, Germany) supplemented with protease inhibitor cocktail (Roche, Germany), and 20 U/ml benzonase (Sigma, Germany). After incubation on ice for 10 min, lysates were sonicated twice for 1 min, cell debris was removed by centrifugation at 70,000 g for 30 min, and lysates were filtered through a 0.45  $\mu$ M filter (Whatman, Maidstone, UK) prior to immunoprecipitation. Samples were immunoprecipitated with a C/EBP $\beta$  antibody mix for 30 min at 4°C (Santa Cruz; C-19 and a customized polyclonal antibody raised against the human recombinant C/EBP $\beta$  protein) and immunoprecipitates were subsequently collected on Protein-G Dynabeads (Novex, Life Technologies). Beads were washed twice in lysis buffer without benzonase, once in lysis buffer without benzonase and NP40, and eluted by incubation with a mix of 6 M urea and 2 M thiourea (Sigma) for 15 min at 25°C. Immunoprecipitation specificities were controlled by immunoprecipitation of SU-DHL1 lysates with nonspecific rabbit IgG control antibodies (Santa Cruz, sc-2017) and subsequent collection on Protein-G Dynabeads.

## **Cell culture, transfection, immunoprecipitation and immunoblotting**

HEKT-293 cells were grown in Dulbecco's modified Eagle medium (DMEM; Invitrogen, USA) and SU-DHL1 cells were grown in RPMI (Invitrogen, USA) supplemented with 10% FCS and 1% penicillin/streptomycin (Invitrogen, USA). Transfection of plasmids in HEKT-293 cells was performed by calcium-phosphate precipitation or Metafectene (Biontex, Munich, Germany) according to the manufacturer's protocol. For validation of PRISMA-identified C/EBP $\beta$  protein interactions, immunoprecipitation of WT or mutant C/EBP $\beta$  proteins expressed in HEKT-293 cells was performed as described previously (Kowenz-Leutz et al, 2010). Briefly, cell lysates were prepared in lysis buffer and immunoprecipitation was performed with appropriate antibodies for 2 h at 4°C. Immunoprecipitated proteins were collected on Protein-G Dynabeads (Novex), separated by SDS-PAGE (NuPAGE, Thermo-Fisher, Waltham, USA) and immunoblots were incubated with appropriate antibodies as indicated and visualized by ECL (GE Healthcare, UK). GST-C/EBP $\beta$  constructs and cloning of mutant C/EBP $\beta$  proteins were as described previously (Kowenz-Leutz et al 1999; 2010 etc). Antibodies were as follows: anti-C/EBP $\beta$  (Leutz lab), anti-C/EBP $\beta$  (Santa Cruz; C-19), anti-Flag (Sigma), anti-HA.11 (Covance), anti-TLE3 (Santa Cruz; sc-9124), anti-WDR77/Mep50 (Biomol; A301-562A), anti-Nup50 (Santa Cruz; sc-133859), anti-Mi2 (Santa Cruz; sc-11378; Santa Cruz; sc-11378), anti-MBD2 (Santa Cruz; sc-12444), anti-MBD3 (Bethyl; A302-538A), anti-PRMT5 (Millipore; 07-405), anti-MTA1 (Biomol; A200-280A), DMAP1 (Santa Cruz; B-10), anti-RbbP4 (Abcam), Stat3 (Cell signaling; 9132P), anti-RelA (Santa Cruz; sc-109, anti-GCN5 (H-75; Santa Cruz; SC-20698), anti-ELL (Bethyl; A301-644A), anti-cyclin T1 (Bethyl; A303-499A-M), anti-CDK9 (Bethyl; A303-493A-M), anti-AF9 (Novus; NB100-1565), anti-MLLT1 (Novus; NBP1-26653), anti-PAF1 (Novus; NB600-274), anti-BRD4 (Bethyl; A301-985A50), anti-AF4 (Santa Cruz; sc-99062), anti-GFP (Roche; 11814460001), anti-SSRP1 (Thermo; PA-22186), anti-SPT16 (Thermo; PA1-12697).

### **In vitro methylation assay**

Peptides, #1-7 (PSL, Heidelberg, Germany) used for in vitro methylation were based on the mouse C/EBP $\beta$  homolog. Peptide sequences are:

#1: MHRLLAWDAASLPPPPAAFRP,

#2: MEVANFYYPDSLAYGAKAARAAPRAAPAAEPAIG,

#3: AAEPAIGEHERAIDFSPYLEPLAPAADFAAPAP,

#4: APHHDFLSDLFADDYGAKPSKPADYGYVSLG,

#5: ADYGYVSLGRAGAKAAPPASFP,

#6: PPAALKAEPGFEPADSKRADDAPAMAAGFPFALRAYLGYQATPSG,

#7: MAAGFPFALRAYLGYQATPSGSSGSLSTSSSSSPPGTPSPDADKA.

Methylation assays were carried out with PRMT4/CARM1 (#51047, BPS Bioscience) in the presence of S-adenosyl-L-(methyl)-3H methionine as methyl donor and incorporation of (3H)-methyl was determined by scintillation counting (Kowenz-Leutz et al 2010).

### **Adipogenesis and RT-PCR analysis**

Adipogenic differentiation was performed with C/EBP $\beta$  WT, R193A,L mutant and TLE3 constructs were transfected into 3T3L1 fibroblasts and cells were grown in the absence of the adipogenic differentiation cocktail (IBMX, Insulin, Dexamethasone) (Kowenz-Leutz et al 2010). Total RNA was isolated (#R1055, Zymo) and cDNA was prepared (#K1622, ThermoScientific). Real-time PCR was performed using SYBR Green (#A25741, Applied Biosystems) and the Quant Studio 6 Flex Cycler (Applied Biosystems). Primers were used as described (Villanueva et al., 2013). Primer sequences: m36B4 forward AGATGCAGCAGATCCGCAT and reverse GTTCTTGCCCATCAGCACC; ADIPOQ forward CCGGAACCCCTGGCAG and reverse

CTGAACGCTGAGCGATACACA; CFD forward CATGCTCGGCCCTACATGG and reverse CACAGAGTCGTCATCCGTCAC; FABP4 forward CACCGCAGACGACAGGAAG and reverse GCACCTGCACCAGGGC.

Adipogenic cell differentiation was visualized after fixation with 4% paraformaldehyde by oil red O staining.

### **Homolog mapping and calculation of overlap with known datasets**

The two Siersbaek interaction datasets (Siersbaek et al., 2011) are based on the mouse homolog of C/EBP $\beta$  and thus all identifiers were mapped to human homologs prior to calculating the overlap between the datasets using the InParanoid Homolog database (<http://inparanoid.sbc.su.se/cgi-bin/index.cgi>). PRISMA data was organized into protein groups reflecting the non-unique mapping of peptides to the protein sequences. Within PRISMA data, the unique IPI identifiers served for overlap calculation. Otherwise, the overlap of a set of protein groups (reference dataset) with another dataset was calculated by determining all mutual UniProt identifiers in the two datasets and projecting them onto the protein groups of the reference dataset.

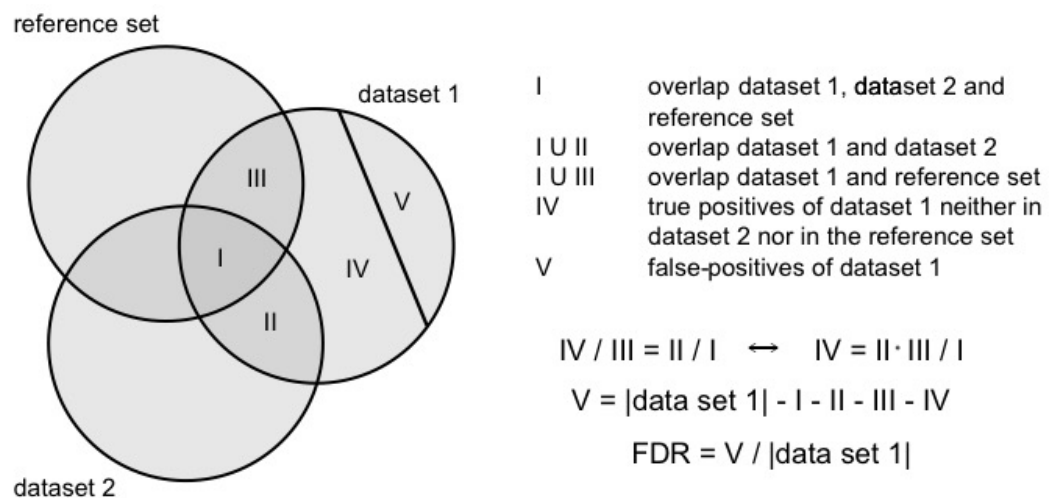
### **Calculations of dataset overlaps**

Overlap of proteins in the full PRISMA dataset (replicates 1 and 2), the PRISMA core interaction set, and the three other datasets (MudPIT HeLa, IP 3T3L1, and IP SU-DHL1) and their union is shown in the following table. Entries in the diagonal capture the total number of proteins in the dataset.

second set reference set	PRISMA SET1+SET2	PRISMA Core interactions	MudPIT HeLa	IP 3TL3L1	IP SU- DHL1	Union HeLa, 3T3L1, SU-DHL
PRISMA SET1+SET2	2363	1302	57	483	1014	1179
PRISMA core interactions	1302	1302	35	390	716	829
MudPIT HeLa	69	46	118	23	43	118
IP 3T3L1	447	372	23	630	349	630
IP SU-DHL1	904	685	41	339	1369	1369
Union (HeLa, 3T3L1, SU- DHL1)	1078	807	118	630	1369	1721

## FDR calculation

To estimate the false discovery rate (FDR) of protein-protein interaction (PPI) data sets, we employed the method proposed by D'haeseleer and Church (2004) which relies on comparing the intersections of two measured datasets with a reference set to approximate the number of false-positive PPIs in the measured datasets (see **figure below**). We thereby assumed that the reference set and the intersection between the two measured datasets is error-free (i.e. they contain no false-positives).



**Scheme S1: Scheme for the calculation of the false discovery rate (FDR) of dataset 1 according to D’haeseleer & Church (2004).** It is assumed that the intersections of the reference set with the datasets (I, III) as well as the intersection between the two datasets (II) are nearly error-free. In addition, the method makes use of the assumption that the reference set overlaps similarly with dataset 1 and dataset 2 (i.e. the relation  $IV / III = II / I$  holds.  $|dataset\ 1|$  denotes the number of proteins in dataset 1.

The assumption that the reference set is error-free can be relaxed since we only need to be sure that it contains no bias in how it intersects with the first and second measured datasets and their intersection [D’haeseleer and Church, 2004]. This can be expected if both measured datasets are obtained using the same measurement method, which is the case for PRISMA SET1 and SET2.

Using the calculation procedure described in **the figure above** for PRISMA SET1 and SET2 with the union of the IP SU-DHL1, IP 3TL3L1 and MudPIT HeLa datasets as reference set, we estimated FDRs of 11.2% and 13.9% for SET1 and SET2, respectively. If using as the two measured datasets the restrictions of SET1 and SET2 to proteins also occurring in the PRISMA core interaction set, the FDRs were reduced to 2.5% ( $SET1 \cap PRISMA$  core interactions) and 3.3% ( $SET2 \cap PRISMA$  core interactions). Overlap counts of the PRISMA sets and the reference set (union of IP SU-DHL1, IP 3TL3L1, MudPIT HeLa) which are needed for FDR calculation (i.e. values for the sizes of areas marked by I, II, III, IV, V in the figure above) are given in the following table.

	Set size	I	II	III	IV	V	FDR
<b>SET1</b>	1896	862	522	186	113	213	11.2%
<b>SET2</b>	1851	862	522	131	79	257	13.9%
<b>SET1 <math>\cap</math> PRISMA core interactions</b>	1203	738	359	51	25	30	2.5%
<b>SET2 <math>\cap</math> PRISMA core interactions</b>	1196	738	359	40	19	40	3.3%

## Ranking of CORUM complexes

We ranked the 1432 complexes obtained from the CORUM database as described in the main text by applying a combination of two criteria: (i) the percentage of proteins of the complex occurring in PRISMA, and (ii) deviation from randomness of the coverage obtained for PRISMA and SU-DHL1. Specifically, for (i), we calculated the percentage for each complex by dividing the number of proteins occurring in the complex from the combined PRISMA replicates 1 and 2 (SET1 + SET2) with matched identifiers using the Perseus tool by the total number of proteins in the complex. For (ii), for each complex, we compared the PRISMA (SU-DHL1) dataset with random protein sets in terms of how many proteins of the complex are covered. Focusing on CORUM data, we considered only the subset of PRISMA and SU-DHL proteins which occurred in the 2678 proteins from the 1432 CORUM complexes, comprising 816 (490) proteins in the PRISMA (SU-DHL) dataset, thus also giving the size of the corresponding random datasets. We first performed the calculations separately for PRISMA and SU-DHL for each of the 1432 complexes. For calculation of a complex of  $C_n > 1$  proteins, of which  $C_p$  proteins with  $0 \leq C_p \leq C_n$  occur in PRISMA, we estimated the probability of observing at least  $C_p$  of  $C_n$  specific proteins within a random set of size  $P_n = 816$  drawn from the total set of  $T_n = 2678$  proteins occurring in any of the CORUM complexes. This is a 'drawing without replacement' scenario (corresponding to the Fisher's exact test), for which success is represented by drawing one of a specific subset (of size  $C_n$ ) of proteins, and thus the probability that at least  $X$  successes are obtained can be calculated as follows:

$$P(X \geq C_p) = \sum_{C=C_p}^{C_n} \frac{\binom{C_n}{C} \binom{T_n - C_n}{P_n - C}}{\binom{T_n}{P_n}}$$

where  $C_n$  is the maximal number of successes (full coverage of a complex of size  $C_n$ ),  $C$  is the number of successes (a minimum of  $C = C_p$  proteins of the complex covered because this is how PRISMA or SU-DHL performed, and a maximum of  $C=C_n$ ),  $T_n = 2678$  (the number of possible results for drawing, which is the number of different proteins in the 1432 CORUM



complexes), and  $P_n$  (the number of draws or size of the random datasets) = 816 (for PRISMA full) and 490 (for SU-DHL1).

For calculation of the probabilities for different complexes, the values of  $C_n$  and  $C_p$ , but not of  $T_n$  and  $P_n$ , can change. The probabilities correspond to a hypergeometric distribution, and we employed the appropriate  $R$  base function (`dhyper`) to compute the values.

The obtained probabilities for each complex, one for PRISMA and one for SU-DHL1, represent how probable it is to obtain the observed (or a more extreme) coverage by chance. We treated the events for PRISMA and SU-DHL1 as independent and multiplied the two probabilities for each complex to obtain the probability that both coverages (or a more extreme) occurred by chance.

We ranked the 1432 complexes based on criterion (i) and (ii) separately. For (i), a high rank corresponded to a high percentage; for (ii), a high rank corresponded to a high significance (i.e. to a low probability; function rank in  $R$ , average values for ties). We computed the final ranking from the sum of the two previous rankings (applying minimal values for ties). The complex list is shown together with the probabilities and rankings in Supplemental Table 5.

## **Bibliography**

Cox, J., and Mann, M. (2008). MaxQuant enables high peptide identification rates, individualized p.p.b.-range mass accuracies and proteome-wide protein quantification. *Nat Biotechnol* 26, 1367-1372.

Cox, J., Neuhauser, N., Michalski, A., Scheltema, R.A., Olsen, J.V., and Mann, M. (2011). Andromeda: a peptide search engine integrated into the MaxQuant environment. *J Proteome Res* 10, 1794-1805.

Csardi G, N.T.T.I., Complex Systems 1695. 2006. <http://igraph.org> (2006). the igraph software package for complex network research., <http://igraph.org>.

D'haeseleer P, Church GM, 2004, Estimating and improving protein interaction error rates. Proceedings of the 2004 IEEE Computational Systems Bioinformatics Conference (CSB 2004), 0-7695-2194-0/04

Kanashova, T., Popp, O., Orasche, J., Karg, E., Harndorf, H., Stengel, B., Sklorz, M., Streibel, T., Zimmermann, R., and Dittmar, G. (2015). Differential proteomic analysis of mouse macrophages exposed to adsorbate-loaded heavy fuel oil derived combustion particles using an automated sample-preparation workflow. *Anal Bioanal Chem* 407, 5965-5976.

Kramer, A., and Schneider-Mergener, J. (1998). Synthesis and screening of peptide libraries on continuous cellulose membrane supports. *Methods Mol Biol* 87, 25-39.

Mudunuri, U., Che, A., Yi, M., and Stephens, R.M. (2009). bioDBnet: the biological database network. *Bioinformatics* 25, 555-556.

Rappsilber, J., Mann, M., and Ishihama, Y. (2007). Protocol for micro-purification, enrichment, pre-fractionation and storage of peptides for proteomics using StageTips. *Nature protocols* 2, 1896-1906.

Szklarczyk, D., Franceschini, A., Wyder, S., Forslund, K., Heller, D., Huerta-Cepas, J., Simonovic, M., Roth, A., Santos, A., Tsafou, K.P., *et al.* (2015). STRING v10: protein-protein interaction networks, integrated over the tree of life. *Nucleic Acids Res* 43, D447-452.

Villanueva, C.J., Vergnes, L., Wang, J., Drew, B.G., Hong, C., Tu, Y., Hu, Y., Peng, X., Xu, F., Saez, E., *et al.* (2013). Adipose subtype-selective recruitment of TLE3 or Prdm16 by PPARgamma specifies lipid storage versus thermogenic gene programs. *Cell Metab* 17, 423-435.

Wickham, H. (2009). *ggplot2. Elegant Graphics for Data Analysis.*